THERMAL AND INERTIAL CORRECTIONS FOR THE HOLE PRESSURE PROBLEM

RADHAKRISHNAN SRINIVASAN

1986

THERMAL AND INERTIAL CORRECTIONS FOR THE HOLE PRESSURE PROBLEM

by

Radhakrishnan Srinivasan

A thesis submitted in partial fulfillment
of the requirements for the degree of

Master of Science in Chemical Engineering

University of Washington
1986

Approved by Bruce A. Finlayson
(Chairperson of Supervisory Committee)

Program Authorized
to Offer Degree Chemical Engineering

Date June 9, 1986

In presenting this thesis in partial fulfillment of the requirements for a Master's degree at the University of Washington, I agree that the Library shall make its copies freely available for inspection. I further agree that extensive copying of this thesis is allowable only for scholarly purposes, consistent with "fair use" as prescribed in the U.S. Copyright Law. Any other reproduction for any purposes or by any means shall not be allowed without my written permission.

Signature S Ratkakrishnan

Date June 9, 1926

University of Washington

Abstract

THERMAL AND INERTIAL CORRECTIONS FOR THE HOLE PRESSURE PROBLEM

by Radhakrishnan Srinivasan

Chairperson of the Supervisory Committee: Professor Bruce A. Finlayson

Dept. of Chemical Engineering

The hole pressure problem is an area of active research in non-Newtonian fluid mechanics, the objective being to relate hole pressure measurements to a property of polymeric liquids known as the first normal stress difference. The present work focuses on the Higashitani-Pritchard theory (HP theory), which is successfully extended to include nonisothermal and inertial effects.

The nonisothermal hole pressure problem is studied computationally for the first time, and the computational results verify the theoretical predictions to within 3% over a wide range of conditions; this indicates that the HP theory is highly successful in predicting the nonisothermal effect.

Inertial effects are included rigorously in the HP theory, also for the first time. The extended HP theory proposed in this work provides conclusive evidence as to the reasons for the failure of the Newtonian hole pressure as a correction factor at higher Reynolds numbers. Hence a computational investigation of the inertial effects is a worthwhile problem for future study.

Table of Contents

List of Figures

List of Tables

Acknowledgement

The author is grateful to Professor Finlayson for having suggested the hole pressure problem as a research topic, and for helpful advice on various aspects of the research presented in this work.

Financial support from the National Science Foundation is gratefully acknowledged.

INTRODUCTION

The hole pressure problem is of current interest in the literature because of a desire to relate the measured hole pressure (P_H) to the first normal stress difference (N_1) of the fluid. Since the problem was first discovered by Broadbent et al. {1} in 1968, there have been several theoretical, numerical and experimental attempts to deduce a relationship between P_H and N_1, and limited success has been achieved under creeping flow conditions and very small Reynolds numbers. The objective of the present work is twofold:

(a) To investigate theoretically and computationally the importance of nonisothermal effects, induced by viscous dissipation, on the hole pressure.

(b) To include inertial effects rigorously in the existing theory, and thus examine the shortcomings in the current technique being used to estimate inertial effects.

Definitions and Notation

Fig.1 shows the flow domain, with fully developed flow existing at the inlet and outlet. The hole pressure (P_H) is defined as the normal thrust at point B minus that at point A:

$$P_H = (P + \tau_{yy})_B - (P + \tau_{yy})_A \qquad [1]$$

The average hole pressure, $P_H(avg)$, is defined as the average normal thrust at the top of the channel (in the hole area) minus that at the bottom of the hole. The notation used is the same as in Bird et al. {2}. P

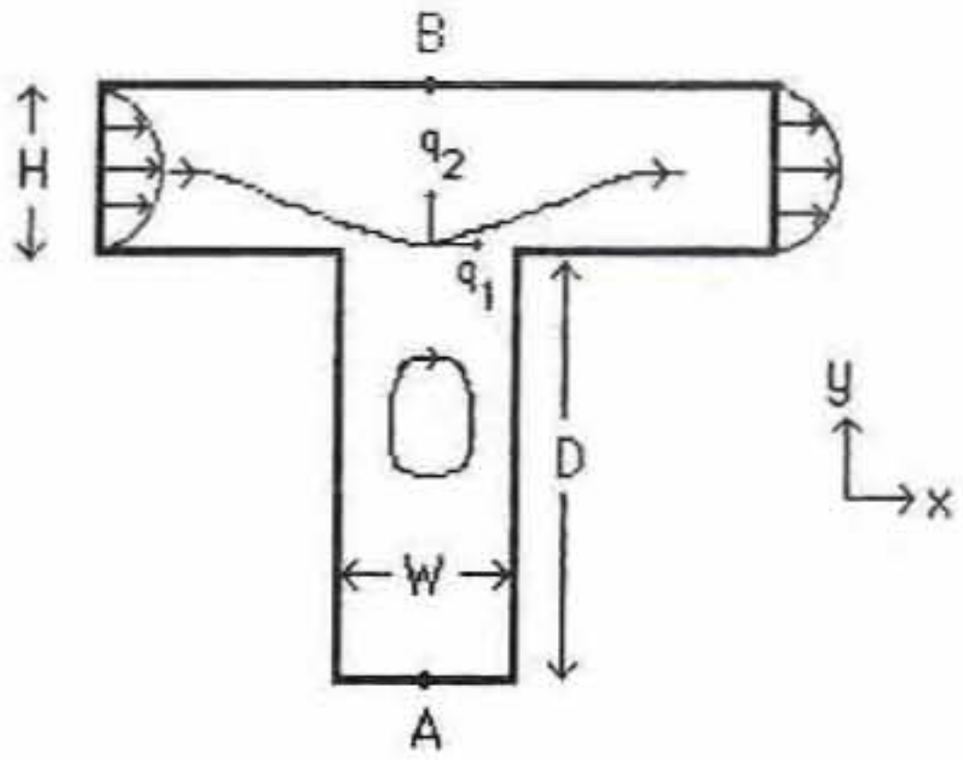

Fig. 1: Transverse slot geometry

is the isotropic pressure, and $\boldsymbol{\tau}$, the extra-stress tensor. The total stress tensor ($\boldsymbol{\pi}$) is defined as :

$$\boldsymbol{\pi} = P\boldsymbol{\delta} + \boldsymbol{\tau} \qquad [2]$$

where $\boldsymbol{\delta}$ is the unit stress tensor.

The x-y-z notation refers to the Cartesian coordinate system, while q_1-q_2-q_3 (and the 1-2-3 subscripts) refer to the orthogonal curvilinear coordinate system (shear coordinates) of ref. {2}.

Hole Pressure Theory

Currently, two theories that relate the hole pressure to the first normal stress difference (N_1) are available: the Tanner-Pipkin theory {3} and the Higashitani-Pritchard (HP) theory {4}. The Tanner-Pipkin theory applies only to the creeping flow of a second-order fluid, and is limited in practical application. Hence the focus of this work is on the HP theory, which is described below.

HP Theory

Higashitani and Pritchard {4} transformed the momentum equation to the shear coordinates of ref. {2}, and deduced the following equation for the hole pressure:

$$P_H = -\int_0^{\tau_B} N_1/2\tau_{12}\, d\tau_{12} \qquad [3]$$

(where $N_1=\tau_{11}-\tau_{22}$, and τ_B is the wall shear stress at point B of fig.1.)
Baird {5} differentiated [3] to obtain the following equation for N_1:

$$N_1 = -2\, dP_H/d\ln\tau_w \qquad [4]$$

where τ_w is the wall shear stress, and N_1 is evaluated at this shear stress. For fluids with N_1 proportional to τ^{n_1}, [3] reduces to :

$$P_H = -N_1/2n_1 \qquad [5]$$

where N_1 is evaluated at the wall shear stress. From [4] and [5], the following equation is obtained:

$$n_1 = d\ln P_H/d\ln\tau_w \qquad [6]$$

Equations [4] and [6] suggest the possibility of using hole pressure measurements to calculate N_1, if the theory is sufficiently accurate. The assumptions used in deriving [3] are the following:

(A_1) Creeping flow exists (the Reynolds number (Re) is very small, so that the inertial terms in the momentum equation are negligible).

(A_2) The velocity field is symmetric about the hole centerline.

(A_3) Unidirectional shear flow exists (and $\partial\tau_{12}/\partial q_1 = 0$) along the hole centerline.

(A_4) $\partial\pi_{11}/\partial q_1 = 0$, along the hole centerline.

When the level of elasticity (as indicated by the Weissenberg number, We) is high, assumptions A_2 and A_3 are questionable; assumption A_4 is definitely not valid for Poiseulle flow (which is driven by a pressure drop) in the channel region, especially towards the top of the channel. However, inspite of the fact that the assumptions of the HP theory are speculative in nature, computational and experimental results in the literature do show that the HP theory is reasonably successful in predicting the hole pressure at low levels of elasticity and creeping flow conditions. A literature survey on the hole pressure computations and experiments can be found in the papers by Webster {6} and Jackson and Finlayson {7}.

In the present work, the HP theory is modified to include nonisothermal effects (under special conditions) and also inertial effects rigorously (i.e., the HP theory is formulated using only assumptions A_2 to A_4). The theoretical and computational results on the nonisothermal hole pressure problem are discussed in chapter I. In chapter II, the inertial correction theory is formulated.

CHAPTER I: THE NONISOTHERMAL HOLE PRESSURE PROBLEM

Problem definition

Fig. 2 shows the domain and boundary conditions.

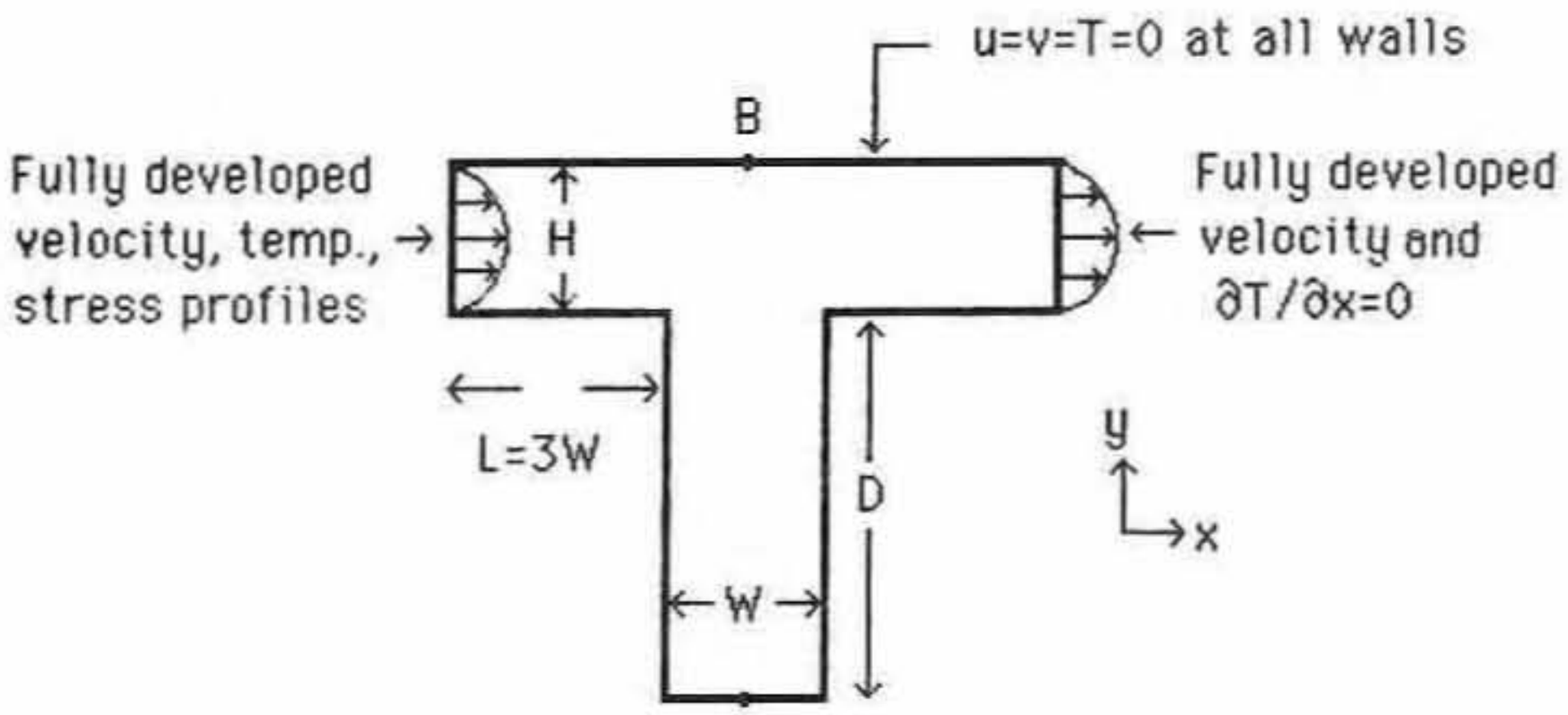

Fig. 2: Boundary conditions for nonisothermal problem

An isothermal boundary condition is imposed at the walls. Fully developed velocity, temperature and stress profiles are imposed at the inlet of the domain. At the outlet, only the fully developed velocity profile is imposed ; a natural boundary condition is used for the temperature. The width of the channel (H) is 1.0 cm, and the width of the hole (W) is 1.0 cm for most of the calculations reported (W/H = 1) and 0.5 cm for a few cases (W/H = 0.5). The entry and exit regions have a length equal to three times the width of the hole; hence for the two geometries studied, the entry and exit regions have lengths of 3 cm (W/H=1) and 1.5 cm (W/H=0.5). This length is considered sufficient for fully developed conditions to exist at the inlet and outlet of the domain (this is justified a posteriori; the computed results show a change of

less than 0.1% and 1% in the velocities and stresses from the inlet to the second (third in case of stresses) row of nodes respectively). The depth of the hole (D) is twice the channel width (H) in all cases; this is sufficient to cause stagnation at the bottom of the channel (ref. {7}, and also from the results obtained in this work).

Discussion of temperature boundary conditions

it is well known that both isothermal and adiabatic boundary conditions (BC) are idealizations difficult to attain in practice. However, in the interest of simplicity, only these BC were considered at the walls of the domain; an isothermal BC was preferred for the reason discussed below.

Because of the isothermal BC imposed at the walls, the inlet and outlet temperature profiles are identical and fully developed. If an adiabatic BC ($\partial T/\partial n=0$, where n is in the direction normal to the boundary) were to be imposed at the walls, there would have to be a net increase in the temperature of the fluid from inlet to outlet because of the heat generated by viscous dissipation (which is the only heat source). However, with adiabatic walls, the specification of the inlet and outlet velocity and temperature profiles poses a difficult problem; the fully developed profiles (which were generated using isothermal walls) cannot be imposed. Nor can a natural BC ($\partial T/\partial n=0$) be used for the temperature at the inlet and outlet, since viscous dissipation causes the temperature of the fluid to keep changing in the axial direction.

Constitutive Equation

The constitutive equation is of the convected Maxwell type, modified to

include shear thinning and temperature dependence of the viscometric functions (the modified White-Metzner model, same as that used by Finlayson and McClelland {9}). The model reproduces experimentally measured temperature dependent viscosity and normal stress data in viscometric flow. The model equation is as follows:

$$\boldsymbol{\tau} + We\,\lambda(\dot{\gamma}, T)\,\boldsymbol{\tau}_{(1)} = -\eta(\dot{\gamma},T)\dot{\boldsymbol{\gamma}} \qquad [1.1]$$

The convected derivative is given by:

$$\boldsymbol{\tau}_{(1)} = \mathbf{v}.\nabla\boldsymbol{\tau} + (\boldsymbol{\omega}.\boldsymbol{\tau} - \boldsymbol{\tau}.\boldsymbol{\omega})/2 - (\dot{\boldsymbol{\gamma}}.\boldsymbol{\tau} + \boldsymbol{\tau}.\dot{\boldsymbol{\gamma}})/2 \qquad [1.2]$$

and the rate of deformation and vorticity tensors are:

$$\dot{\boldsymbol{\gamma}} = \nabla\mathbf{v} + \nabla\mathbf{v}^{*}, \qquad \boldsymbol{\omega} = \nabla\mathbf{v} - \nabla\mathbf{v}^{*} \qquad [1.3]$$

The dimensionless viscosity and time-constant functions are given by:

$$\eta = \eta'(\dot{\gamma}',T')/\eta_0'(T_w') \qquad \lambda = \lambda'(\dot{\gamma}', T')/\lambda_0'(T_w') \qquad [1.4]$$

$\eta_0'(T_w')$ and $\lambda_0'(T_w')$ are the viscosity and time-constant functions evaluated at zero shear rate and wall temperature. All primed quantities are dimensional. The dimensional time-constant function is defined as:

$$\lambda' = \psi_1'(\dot{\gamma}',T')/2\eta'(\dot{\gamma}',T') \qquad [1.5]$$

where Ψ_1' is the primary normal stress coefficient:

$$\Psi_1' = -(\tau'_{11} - \tau'_{22})/\dot{\gamma}'^2 \qquad [1.6]$$

The Weissenberg number (We), appearing in equation [1.1], and the recoverable shear (S_R) (which is a more representative measure of the elasticity than We when there is shear-thinning) are given by the following equations:

$$We = \lambda_0'(T_w') \langle v_x' \rangle / H \qquad [1.7]$$

$$S_R = \Psi_1' \dot{\gamma}'/2\eta' = \lambda'\dot{\gamma}' \qquad [1.8]$$

H is the width of the channel, $\langle v_x' \rangle$ is the average velocity in the channel and $\lambda_0'(T_w')$ is a time constant characteristic of the system. η' and λ' are the viscosity and time-constant functions evaluated at the shear rate $\dot{\gamma}'$, defined in equations [1.4] and [1.5].

Equations of Change

The fluid is assumed to be characterised by constant density (ρ), thermal conductivity (k) and thermal diffusivity (α). The dimensionless momentum and energy equations are:

$$Re\ \mathbf{v}.\nabla\mathbf{v} = -\nabla P - \nabla.\boldsymbol{\tau} \qquad [1.9]$$

$$Pe\ \mathbf{v}.\nabla T = \nabla^2 T - Br\ \boldsymbol{\tau}:\nabla\mathbf{v} \qquad [1.10]$$

Gravitational terms are neglected in the momentum equation. The

equations are nondimensionalised as follows:

$\mathbf{x} = \mathbf{x}'/H \qquad \mathbf{v} = \mathbf{v}'/\langle v_x' \rangle \qquad T = (T'-T_w')/(T_b'-T_w')$

$P = P'H/\eta_0'(T_w')\langle v_x' \rangle \qquad \boldsymbol{\tau} = \boldsymbol{\tau}'H/\eta_0'(T_w')\langle v_x' \rangle$

$Re = \rho\langle v_x' \rangle H/\eta_0'(T_w') \qquad Pe = \langle v_x' \rangle H/\alpha$

$Br = \eta_0'(T_w')\langle v_x' \rangle^2/k(T_b'- T_w')$

Br and Pe are the Brinkman and Peclet numbers respectively. T_b' is a standard temperature defined as:

$T_b' = T_w' + 1 \quad (K)$

Hence the nondimensional temperature (T) represents the actual temperature rise (in K) above the wall temperature.

Fluid Properties

The fluid properties are modelled in the same way as given in ref. {9}:

Viscosity

$$\eta'(\dot{\gamma}', T') = \eta_0'(T')/[1+(\lambda_1'(T')\dot{\gamma}')^2]^{(1-n)/2} \qquad [1.11]$$

where:

$$\lambda_1'(T') = \lambda_1'(T_w') \exp[a_2(1/T'-1/T_w')] \qquad [1.12]$$

$$\eta_0'(T') = \eta_0'(T_w') \exp[a_1(1/T'-1/T_w')] \qquad [1.13]$$

Normal stress coefficient

$$\Psi_1'(\dot{\gamma}', T') = \Psi_{1,0}^{\cdot}(T')/[1+(\lambda_2'(T')\dot{\gamma}')^2]^{(2-n')/2} \qquad [1.14]$$

where:

$$\Psi_{1,0}^{\cdot}(T') = \Psi_{1,0}^{\cdot}(T_w') \exp[a_3(1/T'-1/T_w')] \qquad [1.15]$$

$$\lambda_2'(T') = \lambda_2'(T_w') \exp[a_4(1/T'-1/T_w')] \qquad [1.16]$$

The time-constant of the fluid is given by:

$$\lambda_0'(T_w') = \dot{\Psi}_{1,0}(T_w')/2\eta_0'(T_w') \qquad [1.17]$$

Fluids Used

Nylon-6 is the main fluid used, as in (9).The values of the parameters for nylon-6 are:

Viscosity

$\eta_0'(T_w') = 368.7$ Ns/m^2 a_1=8327 K a_2=17305 K

n=0.7687 $\lambda_1'(T_w')$=0.01766 s

Normal Stress Coefficient

$\dot{\Psi}_{1,0}(T_w') = 12.66$ Ns^2/m^2 a_3=18630 K a_4=5113 K

$n' = 1.201$ $\lambda_2'(T_w') = 0.1455$ s

$\lambda_0'(T_w') = 0.01717$ s

The wall temperature used is T_w' = 535 K throughout. The density (ρ), thermal conductivity (k), and thermal diffusivity (α) are assumed constant at the values available at wall temperature (535 K):

$\rho = 986$ kg/m^3 k=0.25 W/mK $\alpha = 9.6\times10^{-8}$ m^2/s

The time-constant ($\lambda_0'(T_w')$), thermal conductivity and thermal diffusivity were varied to test the effect of We, Br, and Pe respectively on the nonisothermal hole pressure. The viscometric functions were also varied to test the generality of the proposed nonisothermal theory. These

changes are indicated as needed. The Reynolds number (Re) for this fluid is of the order of 10^{-3}, so that the creeping flow assumption of the HP theory (assumption A_1) is essentially satisfied.

Generation of Boundary Conditions

The finite element mesh used is shown in fig. 3 and is the same as that used by Jackson and Finlayson [7]. The fully developed velocity, temperature and stress boundary conditions were generated on a separate rectangular mesh of the same degree of refinement across the channel as at the inlet of the domain shown in fig. 3. The wall temperature used is 535 K. A trial and error procedure was used to generate the boundary conditions, starting from a Newtonian velocity profile as the first guess. With natural boundary conditions being used for the temperature at the inlet and outlet, the velocity boundary conditions were repeatedly updated using the solution from the middle of the rectangular mesh (a more efficient procedure would be to use a long domain and natural BC at the outlet for both velocity and temperature, i.e., to solve the entry length problem). This process was continued until the velocity, temperature and stress profiles did not change to 5 significant digits in the flow direction, and the solution obtained was used as the fully developed boundary conditions.

Proposed Nonisothermal Hole Pressure Theory

The Higashitani-Pritchard theory (equation [3]) predicts the hole pressure under isothermal conditions. For the nonisothermal case with constant wall temperature, the same assumptions (A_1-A_4) as in the isothermal

theory are used. The stress tensor along the hole centerline is assumed to be the same as in unidirectional shear flow, but at different temperatures at each point. This implies that the integral in equation [3] should be evaluated as a line integral, taking into account the changing temperature along the hole centerline. Hence the problem reduces to predicting the temperature profile along the hole centerline. Two approaches are used:

(1) The temperature along the hole centerline is postulated to be the same function of shear stress as in fully developed channel flow, which occurs at the inlet of the domain. By this postulate, the integrand of equation [3] would still be a function of only the shear stress for the nonisothermal case. Hence the following equation is obtained for the nonisothermal hole pressure:

$$P_{H1}(NIT) = -\int_0^{\tau_B\,(NIT)} N_1(\tau_{12}, T(\tau_{12}))/2\tau_{12}\, d\tau_{12} \qquad [1.18]$$

The upper limit of integration is now the wall shear stress at point B corresponding to the nonisothermal case. The isothermal hole pressure ($P_H(T_w)$) is evaluated with the viscometric functions at the wall temperature (T_w), using equation [3] with the upper limit as the wall shear stress at point B corresponding to the isothermal computed solution:

$$P_H(T_w) = -\int_0^{\tau_B(T_w)} N_1(\tau_{12}, T_w)/2\tau_{12}\, d\tau_{12} \qquad [1.19]$$

The correction factor, defined as the ratio of the nonisothermal to the isothermal hole pressures, is given by:

$$CF1 = P_{H1}(NIT)/\ P_H(T_w) \qquad [1.20]$$

CF1 is the theoretical correction factor, using the postulate defined earlier. The upper limits of integration used in the numerator and denominator of [1.20] are the computed wall shear stresses at point B (i.e., the solution from the finite element code VEHEATD), since the theory requires that the actual shear stress at point B be used. However, since it is not clear whether this shear stress is available in practice, results are also reported (as CF1(fd)) using the fully developed wall shear stresses as upper limits in [1.20]. Hence no prior computation is necessary to calculate CF1(fd), which can be used to predict the computed correction factor (CF, defined in equation [1.23]).

The postulate that the temperature along the hole centerline is the same function of shear stress as in fully developed shear flow is not theoretically rigorous. However, it is found to be a reasonable approximation mainly because of the isothermal boundary condition imposed at the walls; with adiabatic walls, the temperatures along the hole centerline would definitely be greater than at the inlet of the domain (due to viscous dissipation), and the longer the inlet region, the greater would be the difference. Higher Peclet numbers also favour a slower rate of change of temperature in the axial direction, which tends to justify the postulate (one calculation is reported for zero Pe; the results indicate that the influence of Pe on the hole pressure is very

small).

(2) A second approach in predicting the nonisothermal effect is to evaluate the integral in [1.18] at an empirically determined average temperature (T_a). The nonisothermal hole pressure according to this definition is given by:

$$P_{H2}(NIT) = -\int_0^{\dot{\gamma}_B(T_W)} N_1(\dot{\gamma},T_a)/2\tau_{12}(\dot{\gamma},T_a)\, d\tau_{12}/d\dot{\gamma}(\dot{\gamma},T_a)\, d\dot{\gamma} \qquad [1.21]$$

The integrand of [1.21] is expressed as a function of shear rate rather than shear stress (so that the integrand can be explicitly evaluated). The upper limit of integration used is the shear rate at point B corresponding to the isothermal solution. The isothermal hole pressure is the same as before, i.e., as given by equation [1.19]. Equivalently, the isothermal hole pressure can be calculated by evaluating the integrand of [1.21] at the wall temperature (T_W). The correction factor according to this definition is:

$$CF2 = P_{H2}(NIT)/\, P_H(T_W) \qquad [1.22]$$

The computed correction factor, CF, is defined as the ratio of the computed nonisothermal to isothermal hole pressures (the word 'computed' is used to denote the finite element solution, generated by the program VEHEATD):

$$CF = P_{H,C}(NIT)/\, P_{H,C}(T_W) \qquad [1.23]$$

The computed isothermal solution is generated at the same average velocity (and hence the same Re and We) as the nonisothermal solution, but with the viscosity and normal stress evaluated at wall temperature only (hence the isothermal solution is generated by setting $a_1=a_2=a_3=a_4=0$ in [1.11]-[1.16]).

The criterion used to fix the average temperature (T_b', used to evaluate the integrand of [1.21]) is that the computed correction factor (CF) match CF2 as closely as possible. The following empirical equation is used to determine the average temperature:

$$T_b' - T_w' = 0.76\,(T_{mix}' - T_w') \qquad [1.24]$$

The primes indicate dimensional values, and T_{mix}' is the mixing cup temperature in fully developed (viscometric) flow, as given by the following equation:

$$T_{mix}' - T_w' = \int_0^{0.5} u(y)T(y)\,dy \;/\; \int_0^{0.5} u(y)\,dy \qquad [1.25]$$

y=0 corresponds to the wall, and y=0.5, to the channel centerline. u(y) and T(y) are the velocity and temperature profiles in fully developed flow. The integration in [1.25] is performed using finite element interpolation (piecewise quadratic) for u(y) and T(y), from the solution at the inlet of the domain (nodes 1-5 in fig. 3).

The factor of 0.76 in [1.24] was fixed by a trial and errror procedure; T_b' was chosen so as to force CF2 to match CF for a test

case, and it was found that the T_s' thus calculated was related to T_{mix}' by [1.24]. For all subsequent calculations, [1.24] was used to calculate T_s' a priori.

An alternative procedure is to calculate an "effective" temperature, T_e', according to the following equation:

$$T_e' - T_w' = 0.7\,(T_{max}' - T_w') \qquad [1.26]$$

T_{max}' is the maximum temperature at the channel centerline in fully developed flow. T_e' could be used in place of T_s' in [1.21]. [1.26] was determined by a similar trial and error procedure to that used in generating [1.24]. For the caiculations reported in this work, both T_s' and T_e' are found to be identical to within two decimal places. However, [1.24] is a more useful equation in that the mixing cup temperature can be measured experimentally, unlike the maximum temperature. Hence T_s' is determined from [1.24], and used in [1.21] and [1.22] to calculate CF2.

The empirically determined CF2 predicts the computed CF to within 1% in most cases; in contrast, CF1, which has more theoretical basis, has a slightly greater error of 1-3%. The impact of mesh refinement on these results, however, needs to be studied. In the next section, numerical results comparing CF, CF1 and CF2 are presented.

Computational and Theoretical Results

Results for nylon-6 and effect of geometry

Table 1 shows the results for nylon-6. Computations were carried out to a maximum recoverable shear (S_R) of 0.21, and a maximum temperature

rise (T_{max}) of 12.3 K at the channel centerline, using the finite element code VEHEATD. This temperature rise causes the viscosity of nylon-6 to drop by a factor of 30% at zero shear rate. Figures 4-7 show the viscosity, normal stress coefficient, shear stress and normal stress respectively for nylon-6, as a function of shear rate and temperature. The isothermal hole pressure is computed with the viscosity and normal stress evaluated at wall temperature only, at all shear rates; the same average velocity, and hence the same Re and We, is used in evaluating the isothermal hole pressure. Figures 8 and 9 show the streamline plots for the isothermal and nonisothermal cases in Table 1, case (c). The corresponding temperature contour and 3-dimensional plots are shown in figures 10 and 11 respectively. The computed correction factor (CF, row 14) is the ratio of the computed nonisothermal to isothermal hole pressures (rows 10 and 9 respectively), as given by [1.23]. CF1 (row 15) is calculated from [1.20], using the nonisothermal and isothermal wall shear stress at point B (rows 12 and 11 respectively) as upper limits. CF1(fd) (row 24) uses the corresponding fully developed wall shear stresses (rows 23 and 22) as the upper limits in [1.20]. CF2 and CF2(fd) (rows 15 and 25) use the isothermal wall shear rate calcuated from the corresponding isothermal shear stresses (rows 11 and 22 respectively) in both the numerator and denominator of [1.22]. The theoretical isothermal hole pressure calculated from equation [1.19] is shown in row 13; a comparison with the computed isothermal hole pressure (row 9) indicates an error of the order of 12%. The average hole pressures are shown in rows 19 and 20; these are calculated by averaging the normal thrust in the hole area. The average hole pressure is much closer to the

theoretical hole pressure than the point value; this is seen from a comparison of rows 9, 13 and 19, and is illustrated in Figure 12. The mixing cup temperature (row 28) is calculated from [1.25] and used in [1.24] to calculate T_s'; row 29, which is the ratio of $(T_e' - T_w')$ to $(T_{mix}' - T_w')$, shows that T_e', calculated from [1.26], is identical to T_s' as given by [1.24], to within two decimal places. Appendix A provides an outline of the numerical integration procedure used in evaluating CF1 and CF2.

The errors between CF and CF1, and CF and CF2 (rows 17, 18 respectively) in Table 1 are of the order of 1-3%, which indicate that CF1 and CF2 are successful in predicting CF. Figure 13 shows a comparison of CF, CF1 and CF2 for nylon-6 (Table 1). CF1(fd) has a slightly greater error (row 26); CF2(fd) is virtually equivalent to CF2, which indicates that CF2 is less sensitive to the upper limits of integration than CF1. Rows 26 and 27 indicate that CF1(fd) and CF2(fd) are successful in predicting CF to within 3% in most cases. Since CF1(fd) and CF2(fd) use the fully developed wall shear stresses as the upper limits in [1.20] and [1.22], no prior computation is necessary to calculate these, unlike CF1 and CF2. The correction factor is also virtually independent of geometry in the range $1/2 \leq W/H \leq 1$, as seen from the results in cases (e) and (f) in Table 1; these should be compared to cases (a) and (c).

Effect of Brinkman number

Table 2 shows the effect of Brinkman number on the nonisothermal hole pressure. The Brinkman number is varied from 8.0 to 16.0, keeping all other parameters constant. This is equivalent to varying the thermal

conductivity of the fluid alone. The viscometric functions used are the same as that of nylon-6, except that the normal stress coefficient is reduced by a constant multiplication factor of 0.87 (i.e., the parameter $\Psi_{1,0}(T_w')$ is specified as 11.012 Ns^2/m^2 instead of 12.66 used for nylon-6; this change was made to obtain easier convergence, but was not necessary). The correction factor drops with increasing Br, because of the increasing temperatures (as seen from row 8). This effect is predicted with remarkable accuracy by both CF1 and CF2; the error is of the order of 1%.

Effect of Peclet and Weissenberg numbers

Table 3 shows the effect of Peclet and Weissenberg numbers. The viscometric functions used are the same as in Table 2. Cases (g) and (l) of Table 3 differ only in the Peclet number (case (g) shown in Table 3 is the same as that shown in Table 2). The effect of a change in Pe from 0 to 7672 is only a 2% increase in the nonisothermal hole pressure; hence the correction factor can be deemed virtually independent of Pe. Cases (m) and (n) of Table 3 should be compared with case (g), Table 3, and case (d), Table 1 respectively; the only change is in the Weissenberg number. The results indicate that changing the Weissenberg number from 0.05 to 0.11 causes CF to change from 0.822 to 0.832, and a change in We from 0.3 to 0.2 changes CF from 0.66 to 0.69. The effect of Weissenberg number is small, within numerical error, but comparison over a wider range is desirable; unfortunately, convergent results could not be obtained at We=0.4.

Viscometric Functions

To ensure that the proposed equations for the nonisothermal hole pressure are not specific to nylon-6, different viscometric functions are considered. According to the HP theory, the nonisothermal hole pressure is lower than the isothermal hole pressure due to two reasons:

(1) The lowering of the integrand in equation [1.18] due to the higher temperatures along the hole centerline.

(2) The lowering of the wall shear stress at point B (τ_B) due to the temperature thinning of viscosity (this lowering occurs because the same average velocity is used in the isothermal and nonisothermal cases).

To check if both phenomena are modelled by equations [1.18] - [1.26], computations were carried out with the following viscometric functions:

(a) The temperature dependence is removed from the viscosity function of nylon-6, but that of the normal stress coefficient is retained, with the following choice of parameters (to be used in [1.11]-[1.14]):

Viscosity

$\lambda_1'(T_w') = 0.01766$ s $\eta_0'(T_w')=368.7$ Ns/m^2

$a_1 = a_2 = 0$, $n = 0.7687$

Normal Stress Coefficient

$\lambda_2'(T_w') = 0.1455$ s $\Psi_1'(T_w') = 11.012$ Ns^2/m^2

$a_3=18630$ K, $a_4=5113$K $n' = 1.201$

The normal stress coefficient is the same as in Tables 2 and 3. Any lowering of the nonisothermal hole pressure in this case must be due to reason (1), i.e., the lowering of the normal stress difference; the viscosity is independent of temperature (the temperature dependence of the normal stress does not have a significant influence on the wall shear stress for the case shown).

(b) The intergrand of [1.18], (N_1/τ_{12}), is made independent of temperature with the following choice of parameters:

Viscosity

$\lambda_1'(T_w')$ = 0.1 s $\quad\quad$ $\eta_0'(T_w')$=368.7 Ns/m^2

a_1=8327 K, a_2=5113 K $\quad\quad$ n = 0.7687

Normal Stress Coefficient

$\lambda_2'(T_w')$ = 0.1 s $\quad\quad$ $\Psi_1'(T_w')$ = 5.006 Ns^2/m^2

a_3=16654 K, a_4=5113K $\quad\quad$ n' = 1.5374

This choice of viscometric functions makes N_1/τ_{12} a function of τ_{12} only, independent of temperature. Appreciably greater shear thinning (as compared to nylon-6) has been introduced, to test the generality of the proposed equations for the nonisothermal hole pressure. Figures 14-17 show the viscosity, normal stress coefficient, shear stress and normal stress as a function of temperature and shear rate for the above choice of parameters. Any lowering of the nonisothermal hole pressure in this case must be purely due to reason (2), i.e., the lowering of the wall shear stress at point B due to the temperature thinning of viscosity.

The results with viscometric functions (a) and (b) are shown in

Table 4 (cases (o) and (p) respectively). CF2 is seen to predict CF to within 1% in both cases, while CF1 has a higher error of 2-3%. Hence the computed results confirm the theoretical predictions.

Mesh Refinement

Finally, it is to be noted that the mesh used in all the simulations (shown in fig. 3) has only one element across the top half of the channel, where there is maximum variation in the temperature and the stresses. For W/H=1, the top half of the channel contributes (as seen computationally) as much as 50% of the total hole pressure. Hence it may be worthwhile to study the effect of mesh refinement in the channel region. However, for W/H=1/2, the top half of the channel contributes only about 10% of the total hole pressure, which indicates that the computed results for this geometry are likely to be more accurate. It is to be noted that the correction factor CF1 is independent of the mesh chosen, unless the upper limit of integration (τ_B) is mesh dependent. CF2, however, was developed using the computed results on this mesh; it is desirable to study the effect of mesh refinement on CF2 (i.e., whether the factor of 0.76 used in [1.24] to calculate the average temperature is satisfactory on a more refined mesh).

In order to test the need for mesh refinement, the finite element code VETIME2D was used to generate the isothermal solution in Table 1, case (c). Figure 18 shows the streamline plot for this case. VETIME2D uses quadratic interpolation for the stresses compared to the linear interpolation used by VEHEATD. Both programs use linear interpolation for the pressure, and quadratic interpolation for the velocity. The results

are as given below:

	VEHEATD	VETIME2D
1. $P_{H,C}(T_w)$	0.5215	0.4641
2. P_H(avg, T_w)	0.5960	0.5566
3. $P_H(T_w)$	0.596	0.596

The results with VETIME2D are significantly different (P_H is lower by about 12%, and P_H(avg) is lower by about 7%). Therefore mesh refinement study is desirable, although it is possible that the ratio of the nonisothermal to isothermal hole pressures (CF) does not change significantly with mesh refinement, even if the individual hole pressures change.

Conclusion

The nonisothermal effect on the hole pressure is significant. For the case of constant wall temperature, constant physical properties (density, thermal conductivity, and thermal diffusivity), fully developed inlet conditions and creeping flow, equations [1.20] and [1.22] predict the computed correction factor satisfactorily (to within 3%), with [1.22] being more accurate (less than 1% error in most cases). The following range of conditions were tested in this work:

$1/2 \leq W/H \leq 1$, $S_R \leq 0.3$, $T_{MAX} \leq 12.3$ K, $0 \leq Pe \leq 12134$

The theory of Higashitani and Pritchard is highly successful in predicting the ratio of the nonisothermal to isothermal hole pressures, although the errors in either of the individual predictions is of the order of 10-30%. The nonisothermal effect is independent of geometry as predicted by the proposed equations, although mesh refinement study is desirable.

Notation Used in Tables 1-4

1.	W/H	Ratio of hole width to channel height
2.	Re	Reynolds number
3.	Pe	Peclet number
4.	Br	Brinkman number
5.	We	Weissenberg number
6.	$S_R(T_W)$	Recoverable shear (isothermal)
7.	S_R(NIT)	Recoverable shear (nonisothermal)
8.	T_{max}	Maximum nondimensional temperature at channel centerline
9.	$P_{H,C}(T_W)$	Computed isothermal hole pressure
10.	$P_{H,C}$(NIT)	Computed nonisothermal hole pressure
11.	$\tau_B(T_W)$	Wall shear stress at point B (fig. 2), isothermal
12.	τ_B(NIT)	Wall shear stress at point B (fig. 2), nonisothermal
13.	$P_H(T_W)$	Theoretical isothermal hole pressure (eqn. [1.19])
14.	CF	Computed correction factor (row 10/row 9, eqn. [1.23])
15.	CF1	Theoretical correction factor (eqn. [1.20])
16.	CF2	Theoretical correction factor (eqn. [i.22])
17.	error1,%	Error between CF and CF1 (rows 14 and 15)
18.	error2,%	Error between CF and CF2 (rows 14 and 16)
19.	P_H(avg,T_W)	Average hole pressure, isothermal
20.	P_H(avg,NIT)	Average hole pressure, nonisothermal
21.	T_p (= T_p' - T_w', K)	Peak nondimensional temperature occuring at nodes 152 and 168 (in fig. (3)) for all cases with W/H=1, except for case (l) where the peak occurs at node 160. For W/H=1/2 (table 1(e) and (f)), the peak occurs at nodes 144 and 176.
22.	τ_W(fd,T_W)	Fully developed isothermal wall shear stress
23.	τ_W(fd,NIT)	Fully developed nonisothermal wall shear stress
24.	CF1(fd)	Theoretical correction factor using fully developed stresses in rows 23 and 22 as upper limits in numerator and denominator of [1.20] respectively.
25.	CF2(fd)	Theoretical correction factor using wall shear rate calculated from row 22 as upper limit in numerator and denominator of [1.22].
26.	error1(fd),%	Error between CF and CF1(fd).
27.	error2(fd),%	Error between CF and CF2(fd).
28.	T_{mix}(=T_{mix}'-T_w', K)	Nondimensional mixing cup temperature in fully developed (viscometric) flow.
29.	T_e/T_{mix} (= (T_e' - T_w')/T_{mix})	Ratio of nondimensional effective to mixing cup temperatures; T_e' as calculated from [1.26].

Table 1: Computed and Theoretical Results for Nylon-6

Case:	(a)	(b)	(c)	(d)	(e)	(f)
1. W/H	1	1	1	1	1/2	1/2
2. Re	0.0014	0.0017	0.002	0.0031	0.0014	0.002
3. Pe	5425	6644	7672	12134	5425	7672
4. Br	4.0	6.0	8.0	20.0	4.0	8.0
5. We	0.0894	0.1095	0.1265	0.20	0.0894	0.1265
6. $S_R(T_W)$	0.163	0.174	0.181	0.212	0.163	0.181
7. S_R(NIT)	0.160	0.169	0.175	0.193	0.160	0.175
8. T_{max}	2.837	4.162	5.458	12.342	2.837	5.458
9. $P_{H,C}(T_W)$	0.465	0.500	0.522	0.565	0.537	0.593
10. $P_{H,C}$ (NIT)	0.419	0.432	0.435	0.391	0.483	0.492
11. $\tau_B(T_W)$	4.897	4.859	4.825	4.671	5.654	5.562
12. τ_B (NIT)	4.690	4.567	4.464	3.949	5.424	5.163
13. $P_H(T_W)$	0.530	0.569	0.596	0.674	0.650	0.724
14. CF	0.900	0.864	0.833	0.692	0.899	0.830
15. CF1	0.909	0.870	0.837	0.672	0.915	0.847
16. CF2	0.901	0.862	0.826	0.663	0.903	0.829
17. error1, %	1.0	0.69	0.48	-2.9	1.8	2.0
18. error2, %	0.11	-0.23	-0.84	-4.2	0.44	-0.12
19. P_H(avg,T_W)	0.529	0.570	0.596	0.666	0.574	0.647
20. P_H(avg,NIT)	0.473	0.487	0.488	0.434	0.514	0.528
21. T_p	2 981	4.382	5.755	13.02	2.920	5.620
22. τ_W(fd,T_W)	5.876	5.827	5.782	5.569	5.876	5.827
23. τ_W(fd,NIT)	5.631	5.482	5.356	4.726	5.631	5.482
24. CF1(fd)	0.915	0.879	0.848	0.691	0.915	0.879
25. CF2(fd)	0.903	0.865	0.830	0.669	0.903	0.865
26. error1(fd), %	1.63	1.68	1.77	-0.14	1.63	1.68
27. error2(fd), %	-0.33	0.11	-0.36	-3.32	-0.33	0.11
28. T_{mix}	2.607	3.826	5.021	11.39	2.607	5.021
29. T_e/T_{mix}	0.762	0.761	0.761	0.759	0.762	0.761

Table 2: Effect of Brinkman Number

	Case:	(g)	(h)	(i)	(j)	(k)
1.	W/H	1	1	1	1	1
2.	Re	0.002	0.002	0.002	0.002	0.002
3.	Pe	7672	7672	7672	7672	7672
4.	Br	8.0	10.0	12.0	14.0	16.0
5.	We	0.11	0.11	0.11	0.11	0.11
6.	$S_R(T_W)$	0.157	0.157	0.157	0.157	0.157
7.	S_R(NIT)	0.152	0.151	0.150	0.148	0.147
8.	T_{max}	5.458	6.714	7.960	9.178	10.369
9.	$P_{H,C}(T_W)$	0.456	0.456	0.456	0.456	0.456
10.	$P_{H,C}$ (NIT)	0.379	0.362	0.347	0.333	0.318
11.	$\tau_B(T_W)$	4.833	4.833	4.833	4.833	4.833
12.	τ_B (NIT)	4.470	4.379	4.299	4.222	4.148
13.	$P_H(T_W)$	0.519	0.519	0.519	0.519	0.519
14.	CF	0.832	0.794	0.761	0.729	0.698
15.	CF1	0.837	0.801	0.769	0.739	0.711
16.	CF2	0.826	0.790	0.756	0.725	0.694
17.	error1, %	0.60	0.88	1.05	1.37	1.86
18.	error2, %	-0.84	-0.5	-0.66	-0.55	-0.57
19.	P_H(avg,T_W)	0.525	0.525	0.525	0.525	0.525
20.	P_H(avg,NIT)	0.428	0.401	0.390	0.372	0.356
21.	T_p	5.751	7.068	8.374	9.648	10.890
22.	τ_W(fd,T_W)	5.782	5.782	5.782	5.782	5.782
23.	τ_W(fd,NIT)	5.356	5.249	5.155	5.065	4.978
24.	CF1(fd)	0.848	0.814	0.783	0.755	0.728
25.	CF2(fd)	0.829	0.794	0.761	0.730	0.700
26.	error1(fd), %	1.92	2.52	2.89	3.57	4.30
27.	error2(fd), %	-0.36	0.0	0.0	0.14	0.29
28.	T_{mix}	5.021	6.180	7.333	8.460	9.563
29.	T_e/T_{mix}	0.761	0.760	0.760	0.759	0.759

Table 3: Effect of Peclet and Weissenberg Numbers

	Case:	(g)	(l)	(m)	(n)
1.	W/H	1	1	1	1
2.	Re	0.002	0.002	0.002	0.0031
3.	Pe	7672	0	7672	12134
4.	Br	8.0	8.0	8.0	20.0
5.	We	0.11	0.11	0.05	0.30
6.	$S_R(T_W)$	0.157	0.157	0.072	0.318
7.	S_R(NIT)	0.152	0.152	0.069	0.290
8.	T_{max}	5.458	5.458	5.458	12.342
9.	$P_{H,C}(T_W)$	0.456	0.456	0.211	0.880
10.	$P_{H,C}$ (NIT)	0.379	0.372	0.174	0.576
11.	$\tau_B(T_W)$	4.833	4.833	4.859	4.625
12.	τ_B (NIT)	4.470	4.434	4.486	3.932
13.	$P_H(T_W)$	0.519	0.519	0.238	0.998
14.	CF	0.832	0.816	0.822	0.655
15.	CF1	0.837	0.827	0.834	0.677
16.	CF2	0.826	0.826	0.827	0.663
17.	error1, %	0.60	1.35	1.46	3.36
18.	error2, %	-0.84	1.2	0.6	1.2
19.	P_H(avg,T_W)	0.525	0.525	0.246	0.955
20.	P_H(avg,NIT)	0.428	0.423	0.199	0.627
21.	T_p	5.751	7.268	5.721	13.02
22.	τ_W(fd,T_W)	5.782	5.782	5.782	5.569
23.	τ_W(fd,NIT)	5.356	5.356	5.356	4.726
24.	CF1(fd)	0.848	0.848	0.848	0.691
25.	CF2(fd)	0.829	0.829	0.829	0.670
26.	error1(fd), %	1.92	3.92	3.16	5.50
27.	error2(fd), %	-0.36	1.59	0.85	2.29
28.	T_{mix}	5.021	5.021	5.021	11.386
29.	T_e/T_{mix}	0.761	0.761	0.761	0.759

Table 4: Effect of Viscometric Functions

	Case:	(o)	(p)
1.	W/H	1	1
2.	Re	0.002	0.002
3.	Pe	7672	7672
4.	Br	8.0	8.0
5.	We	0.11	0.05
6.	$S_R(T_W)$	0.157	0.230
7.	S_R(NIT)	0.153	0.216
8.	T_{max}	5.727	4.176
9.	$P_{H,C}(T_W)$	0.456	0.286
10.	$P_{H,C}$ (NIT)	0.365	0.247
11.	$\tau_B(T_W)$	4.833	3.930
12.	τ_B (NIT)	4.849	3.707
13.	$P_H(T_W)$	0.519	0.386
14.	CF	0.801	0.865
15.	CF1	0.772	0.890
16.	CF2	0.809	0.864
17.	error1, %	-3.7	2.89
18.	error2, %	0.97	-0.12
19.	P_H(avg,T_W)	0.525	0.347
20.	P_H(avg,NIT)	0.419	0.299
21.	T_p	6.034	4.374
22.	τ_W(fd,T_W)	5.782	4.518
23.	τ_W(fd,NIT)	5.782	4.263
24.	CF1(fd)	0.802	0.890
25.	CF2(fd)	0.810	0.864
26.	error1(fd), %	0.12	2.89
27.	error2(fd), %	1.12	-0.12
28.	T_{mix}	5.252	3.834
29.	T_e/T_{mix}	0.763	0.762

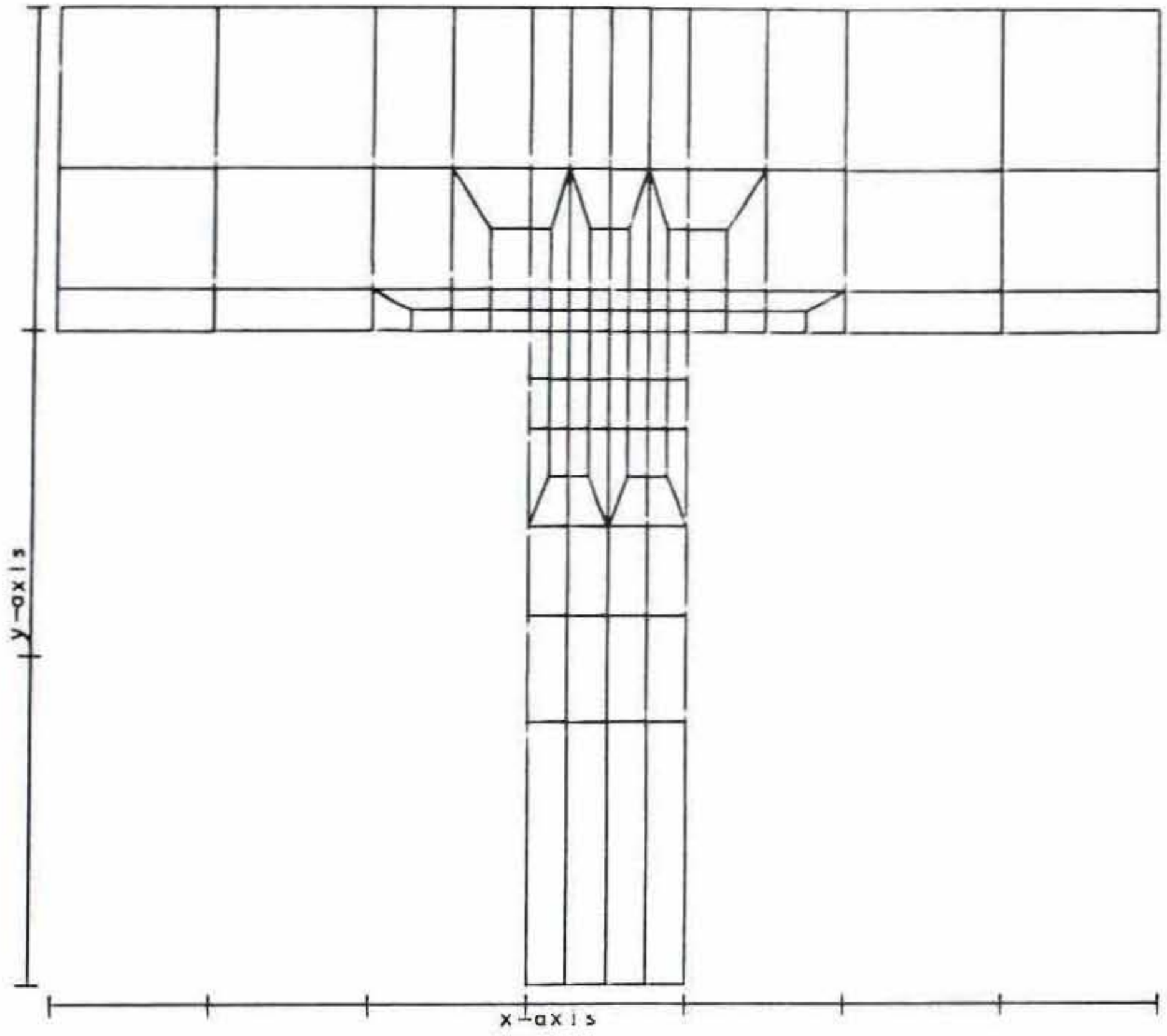

Fig. 3: Mesh used

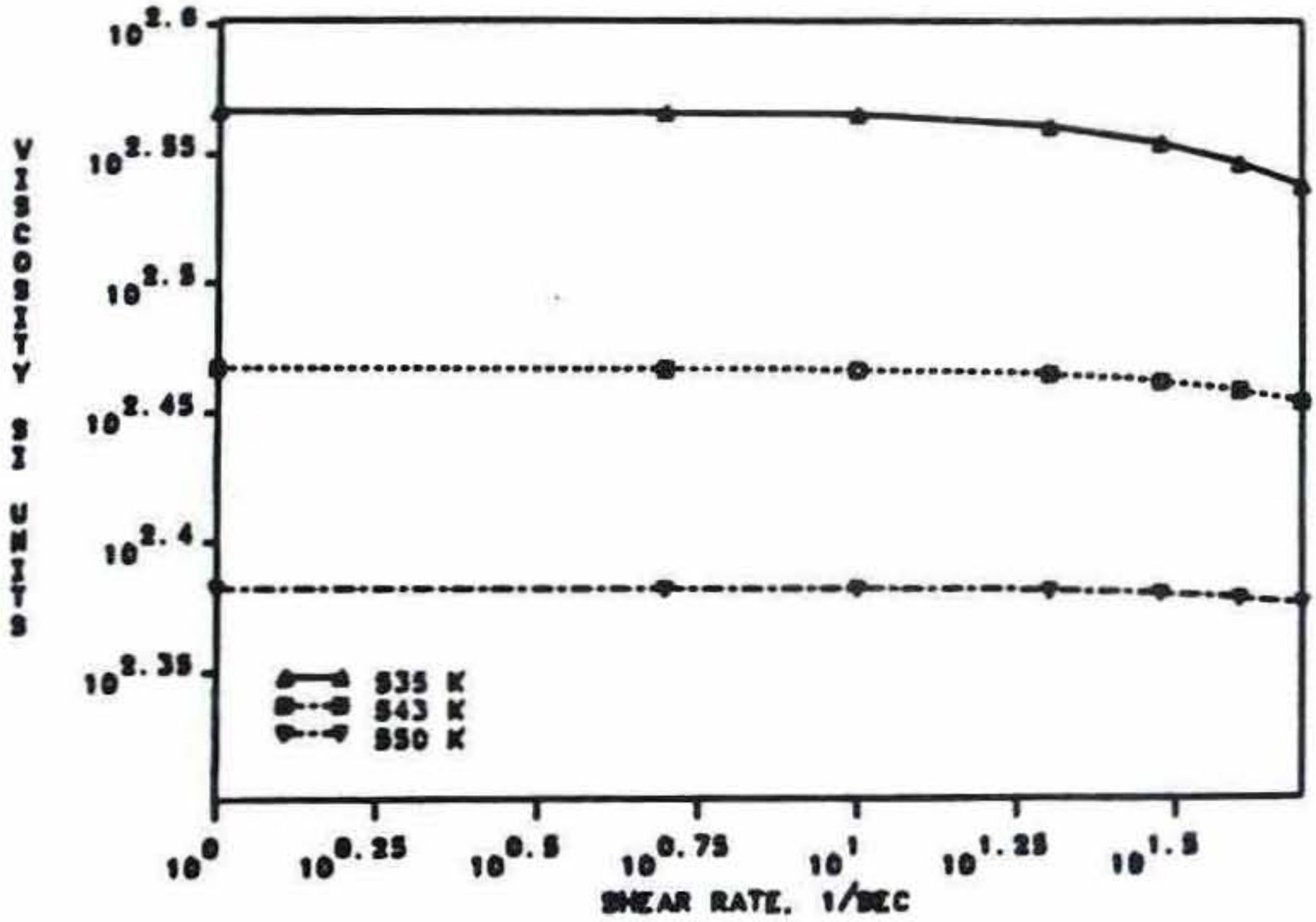

Fig. 4: Viscosity, Nylon-6

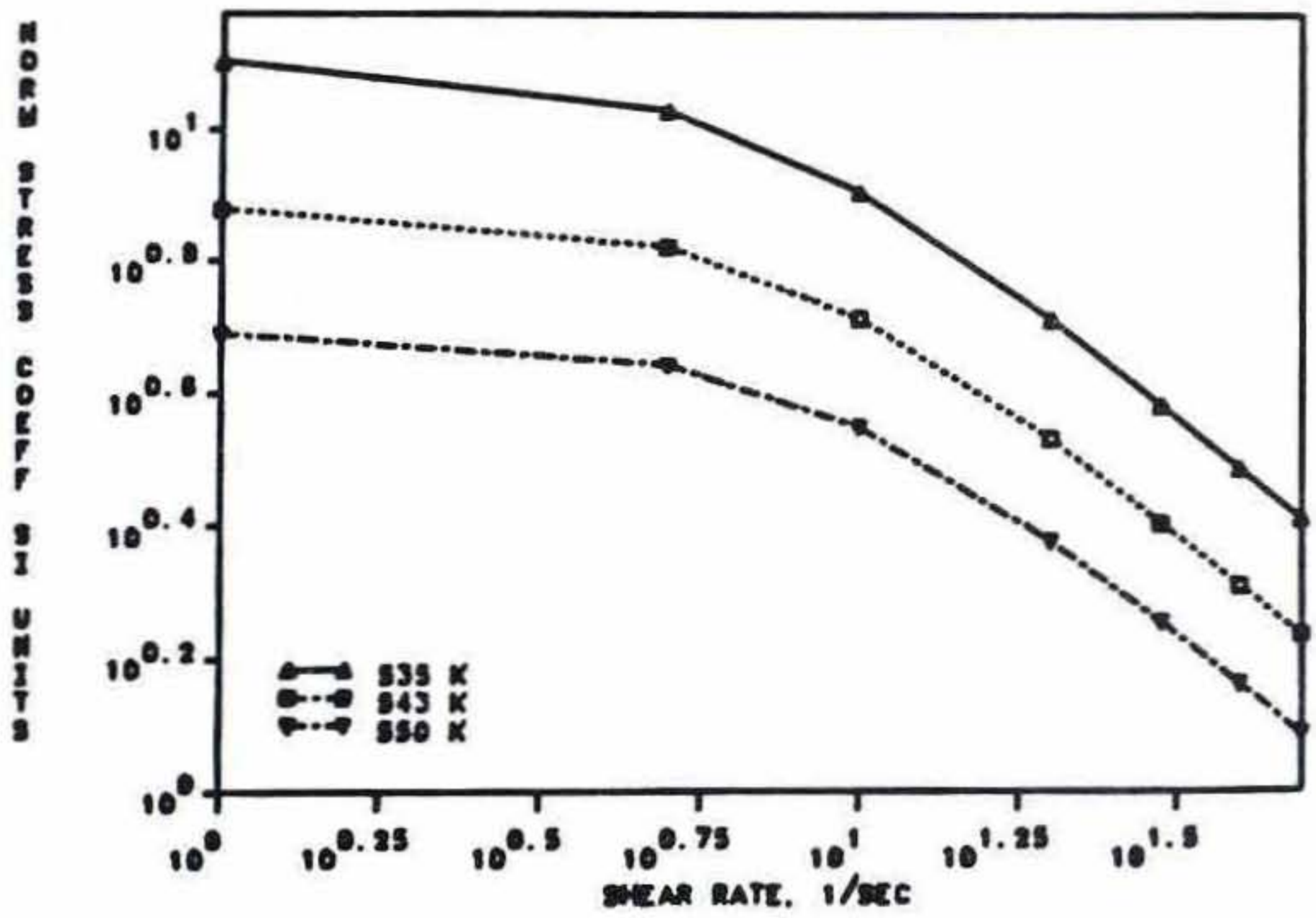

Fig. 5: Normal stress coeff., Nylon-6

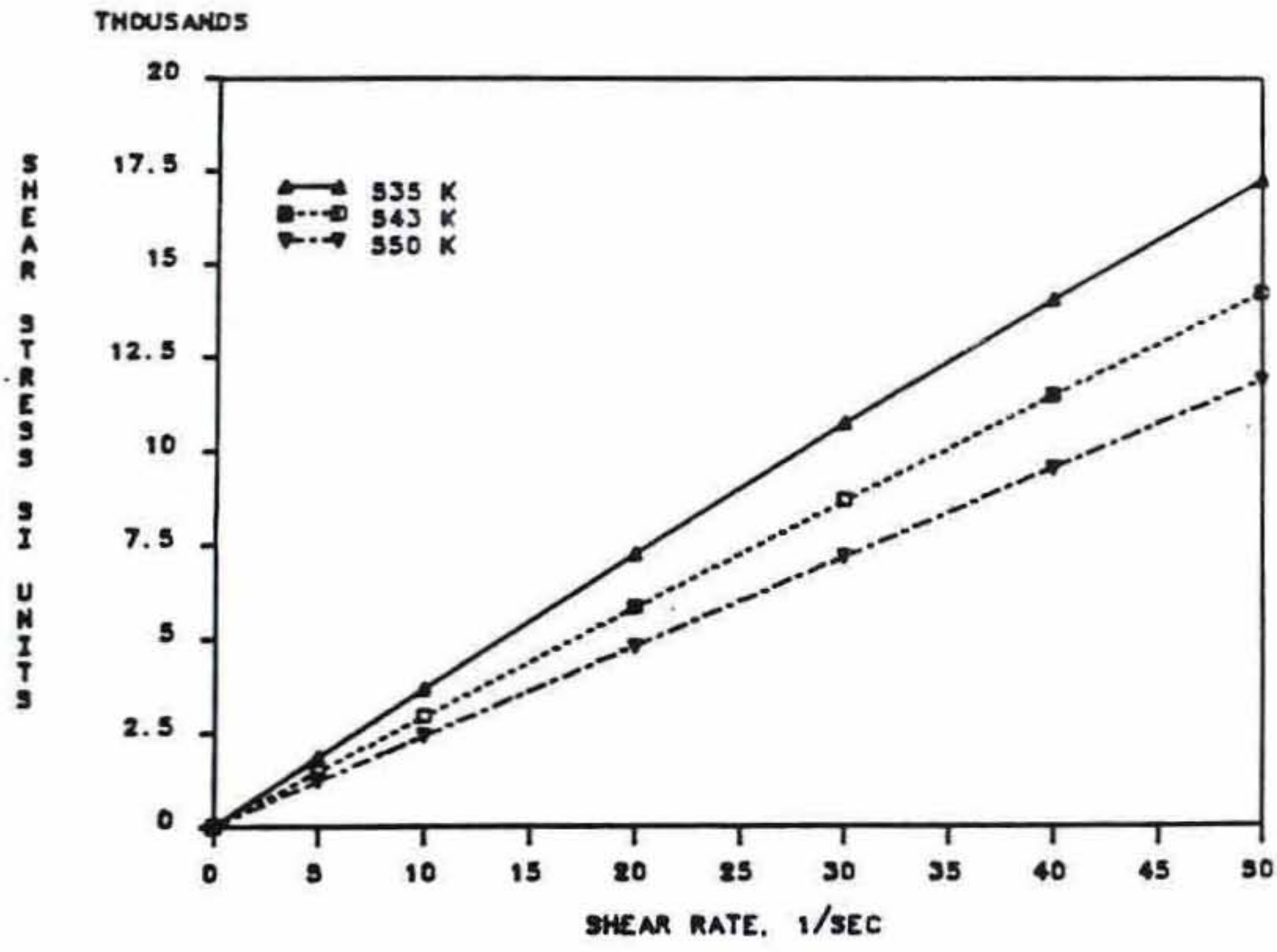

Fig. 6: Shear stress, Nylon-6

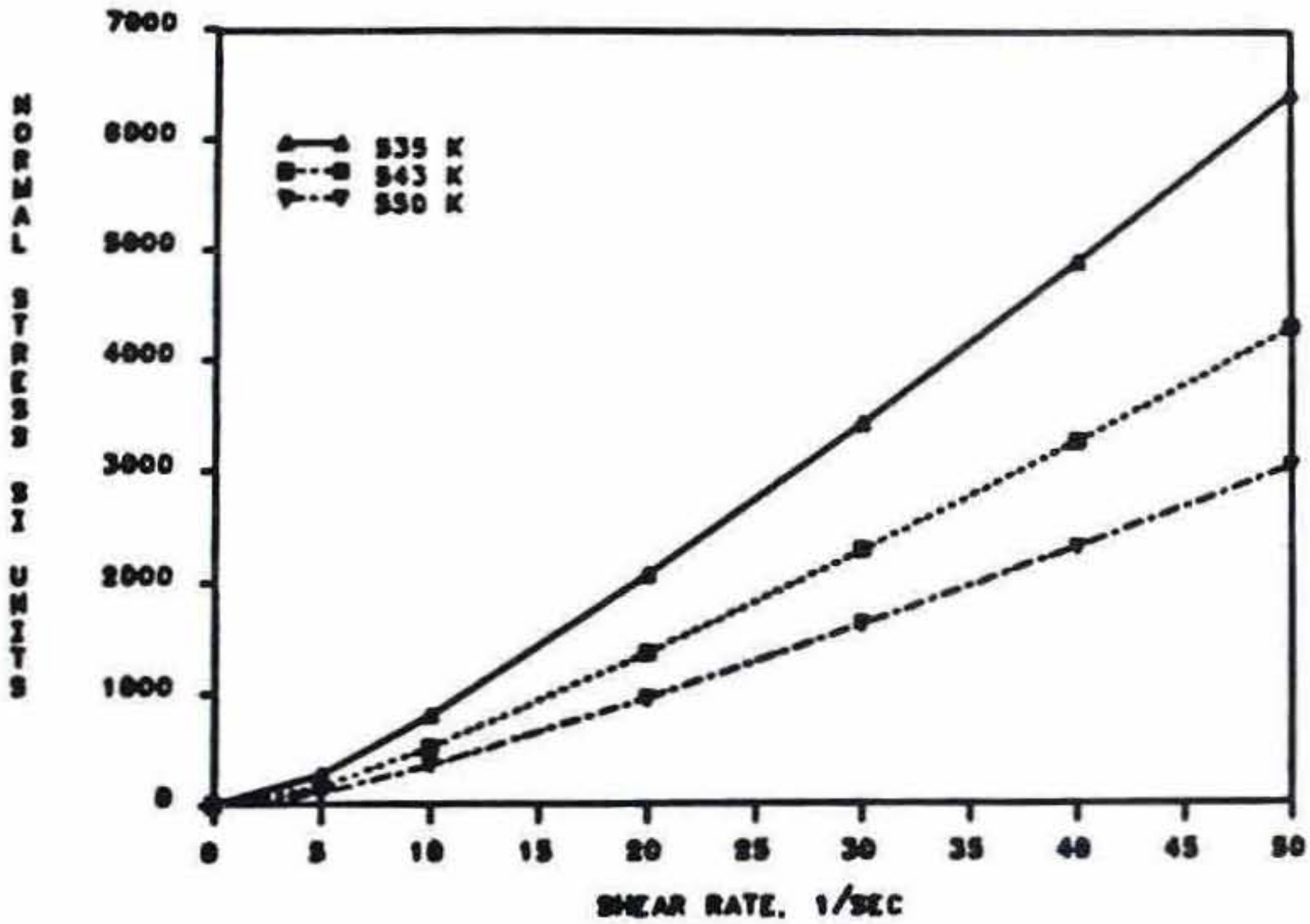

Fig. 7: Normal stress, Nylon-6

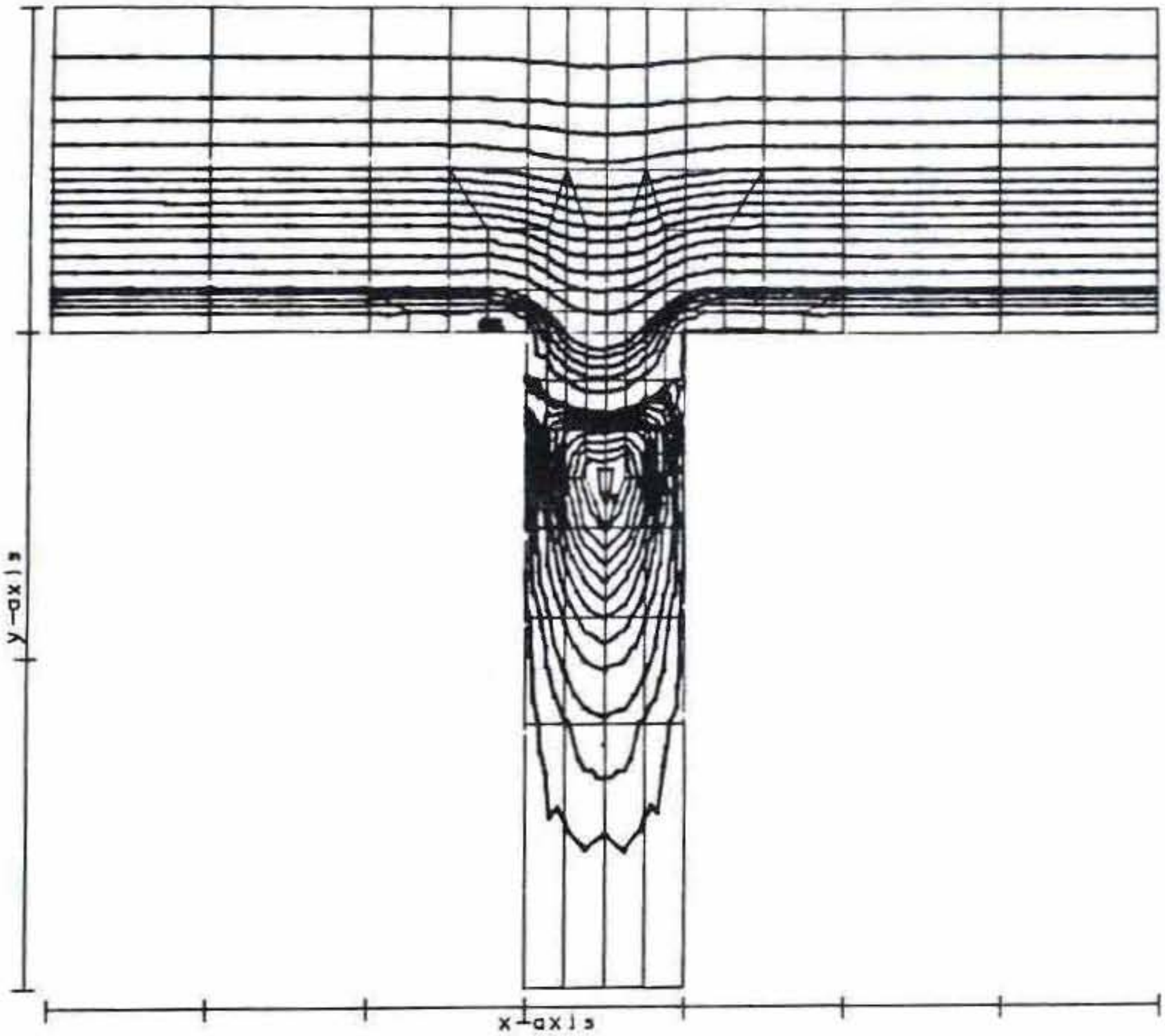

Fig. 8: Streamlines, isothermal, case (c)

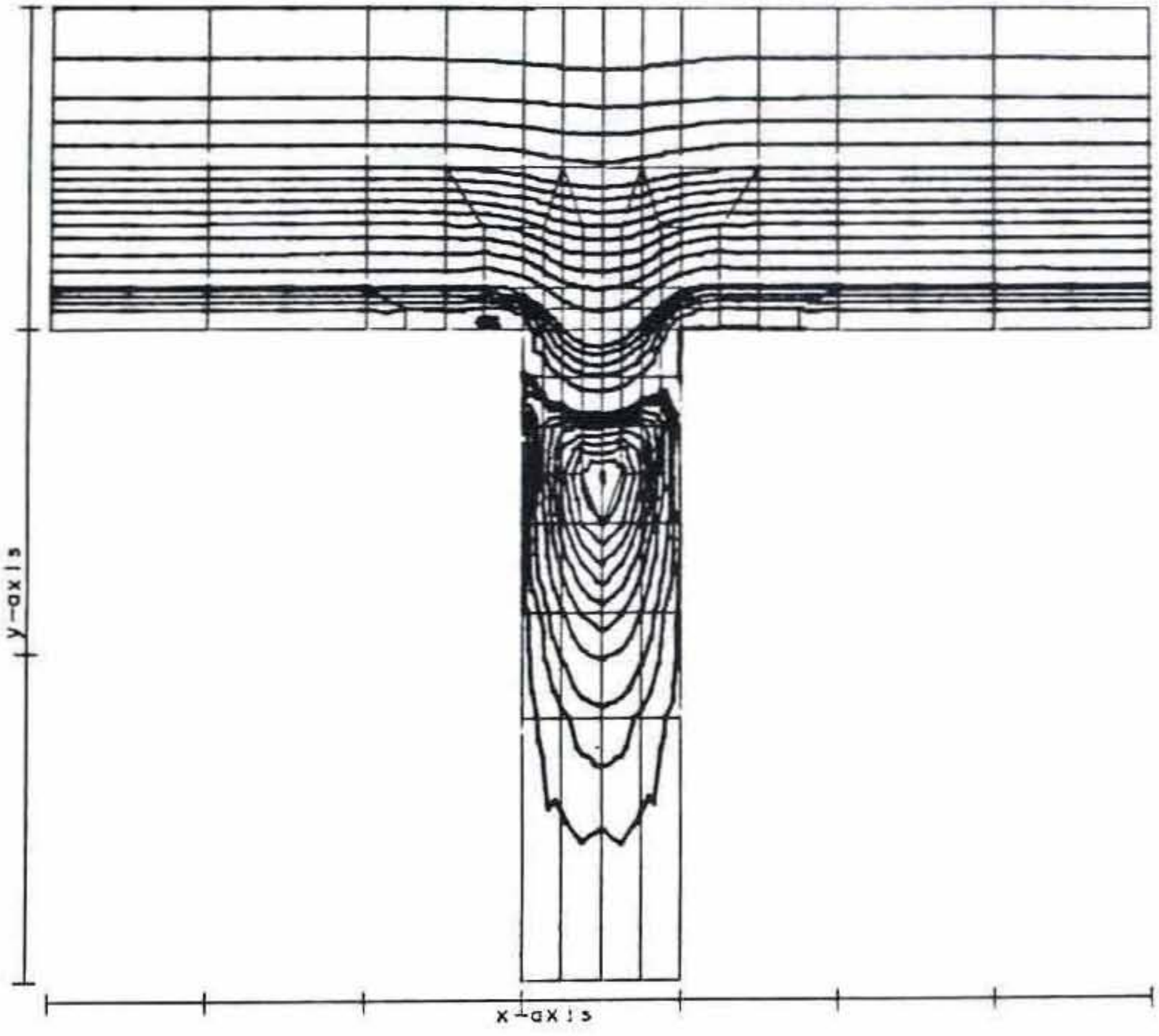

Fig. 9: Streamlines, nonisothermal, case (c)

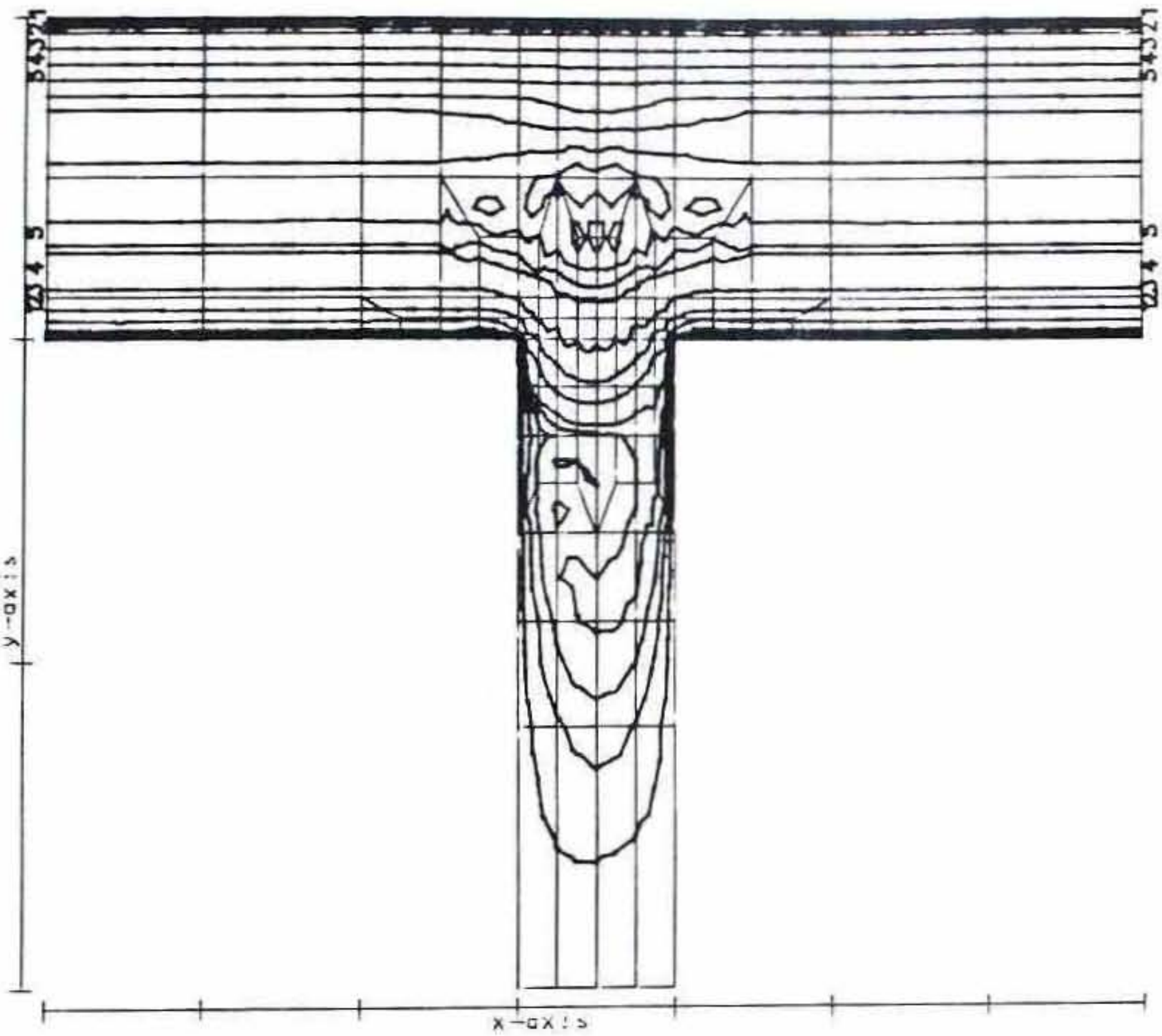

Fig. 10: Temperature contours, case (c)

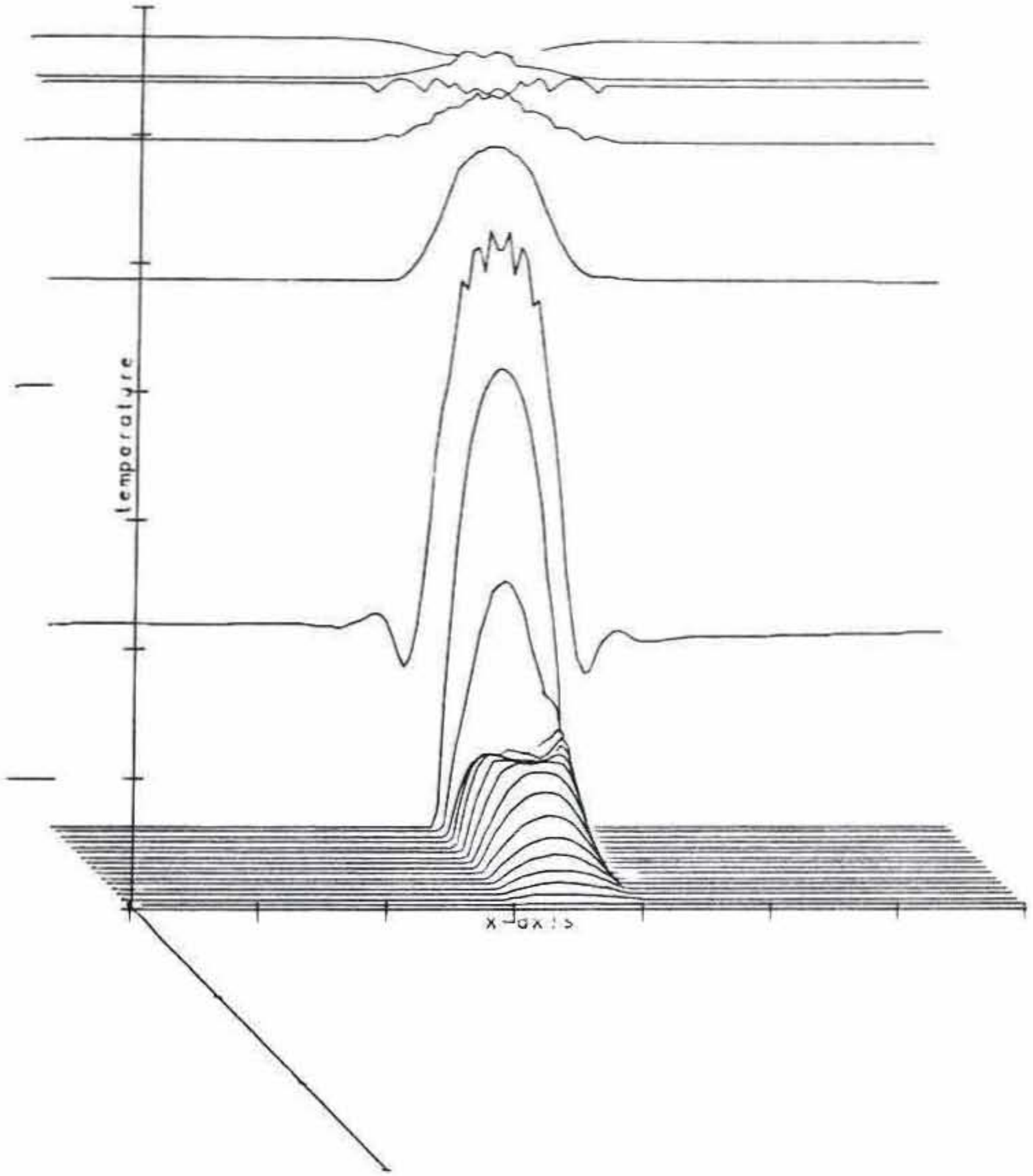

Fig. 11: 3-D Temperature plot, case (c)

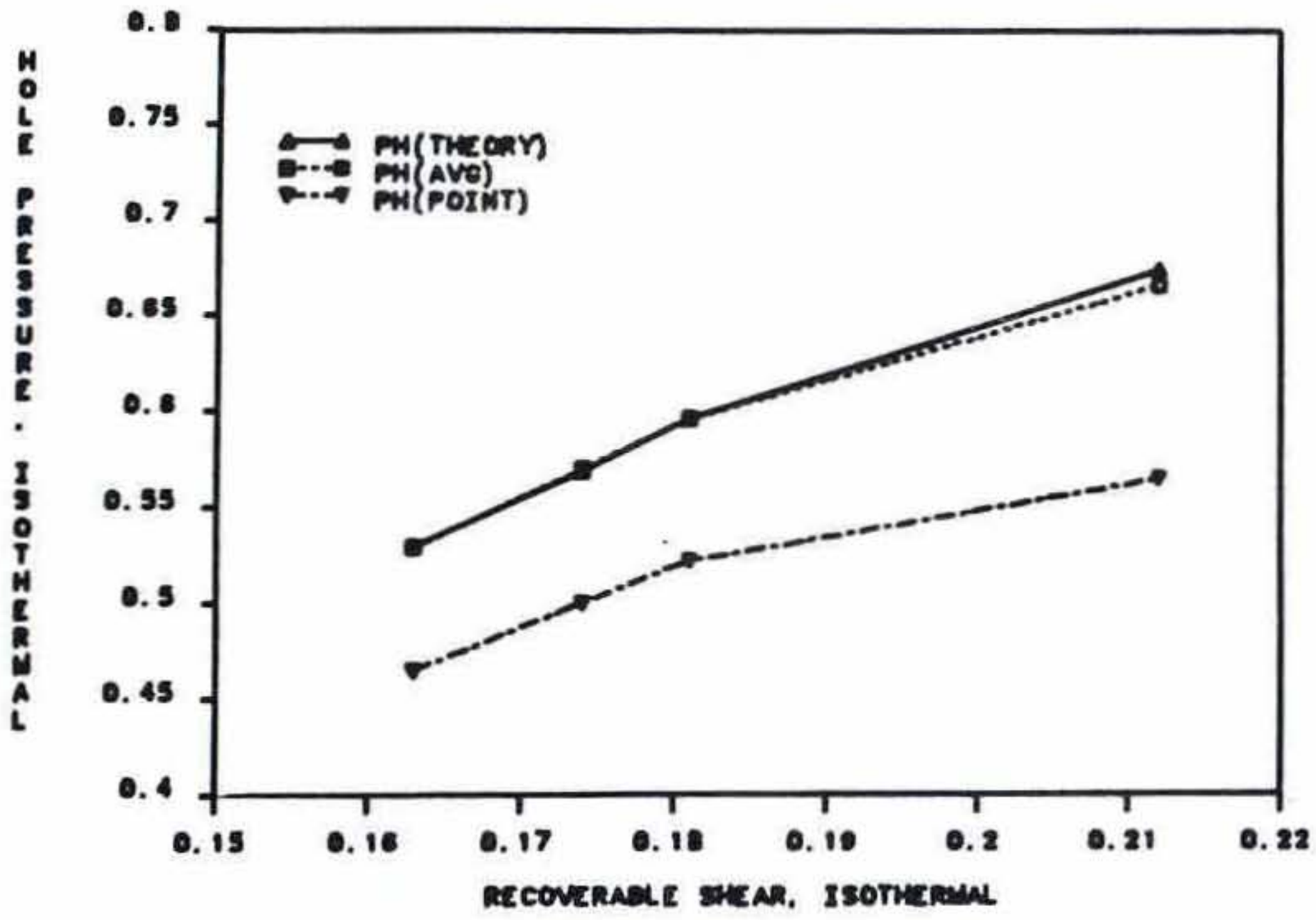

Fig. 12: Average and point P_H, Nylon-6, W/H=1

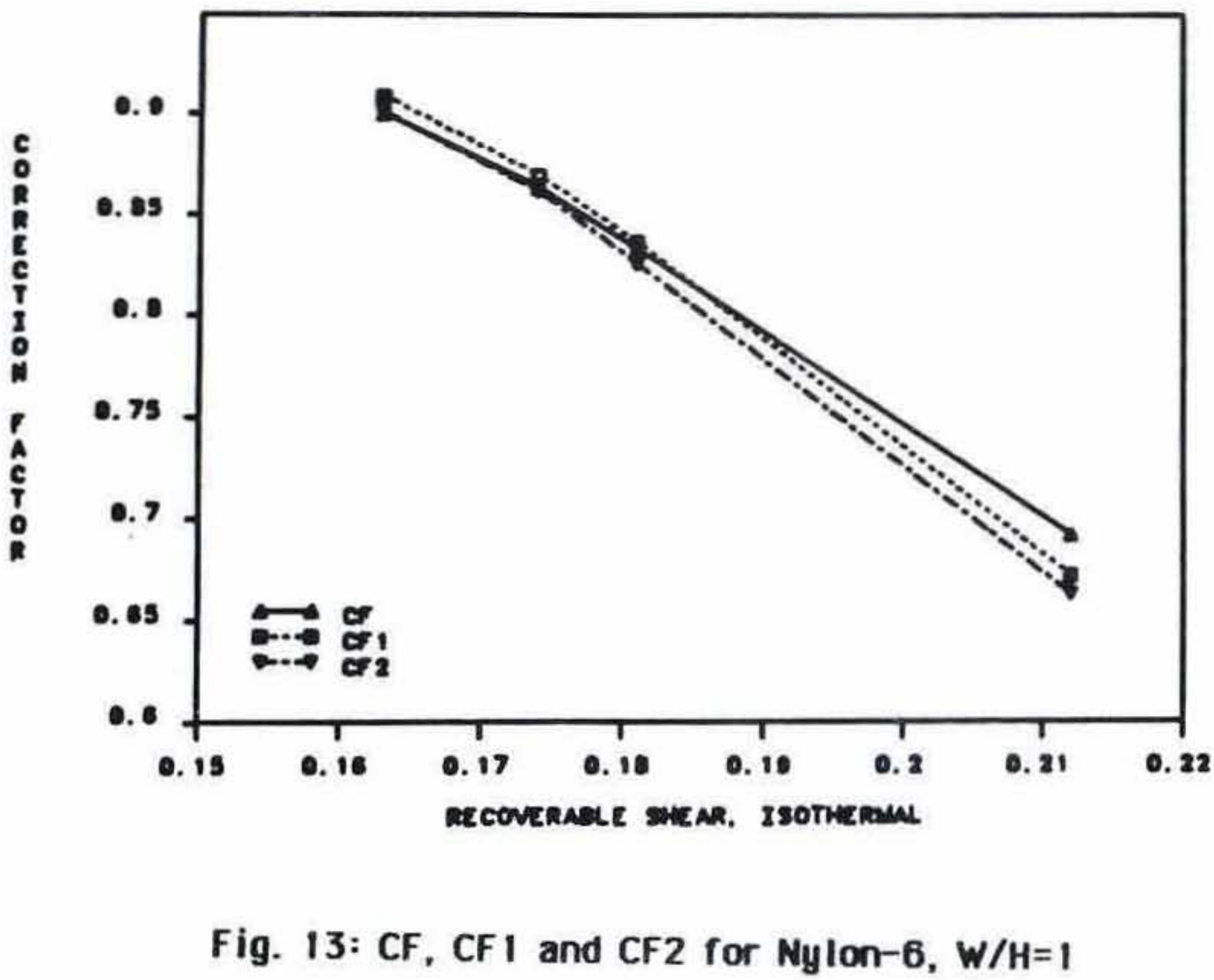

Fig. 13: CF, CF1 and CF2 for Nylon-6, W/H=1

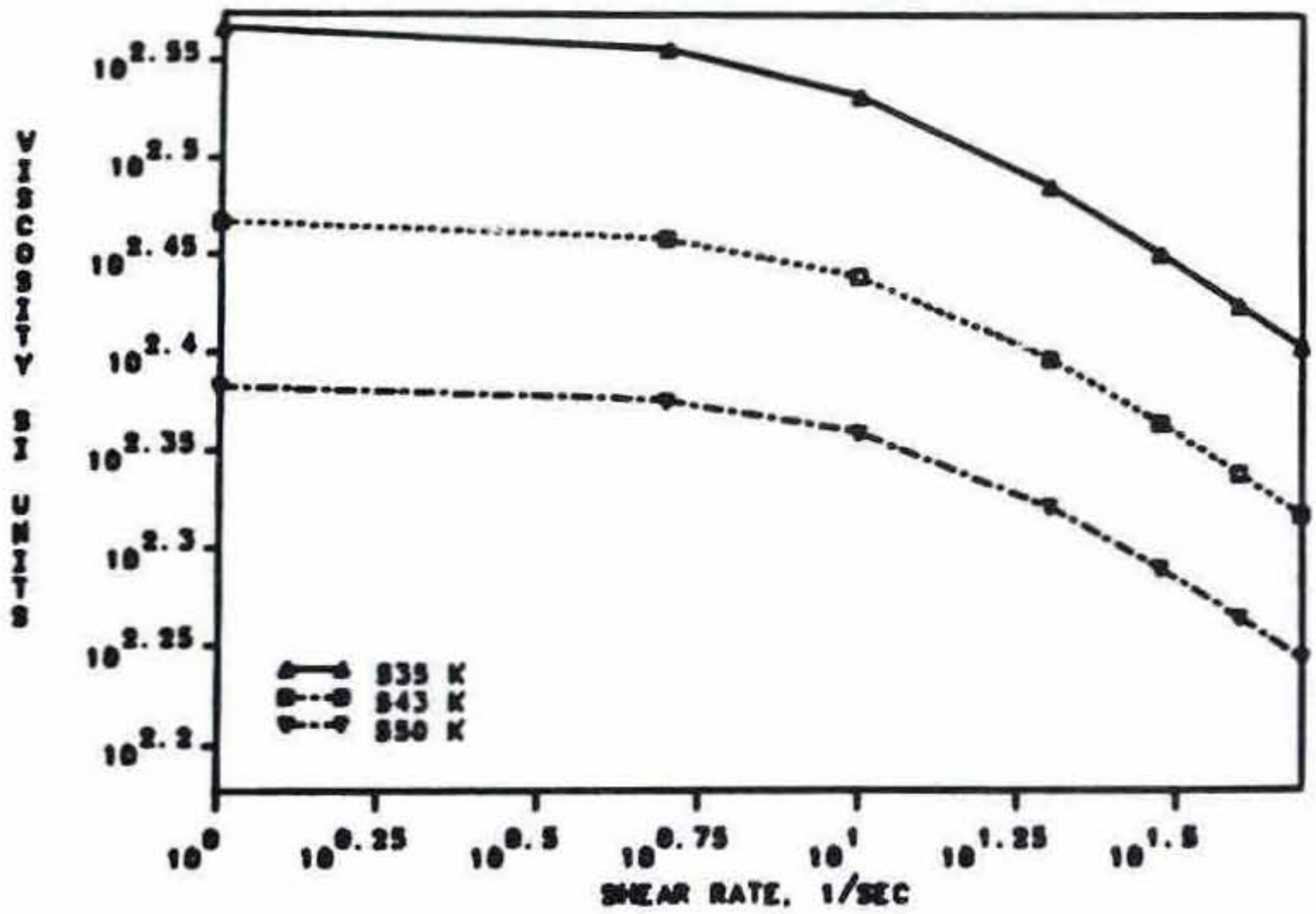

Fig. 14: Viscosity, case (p)

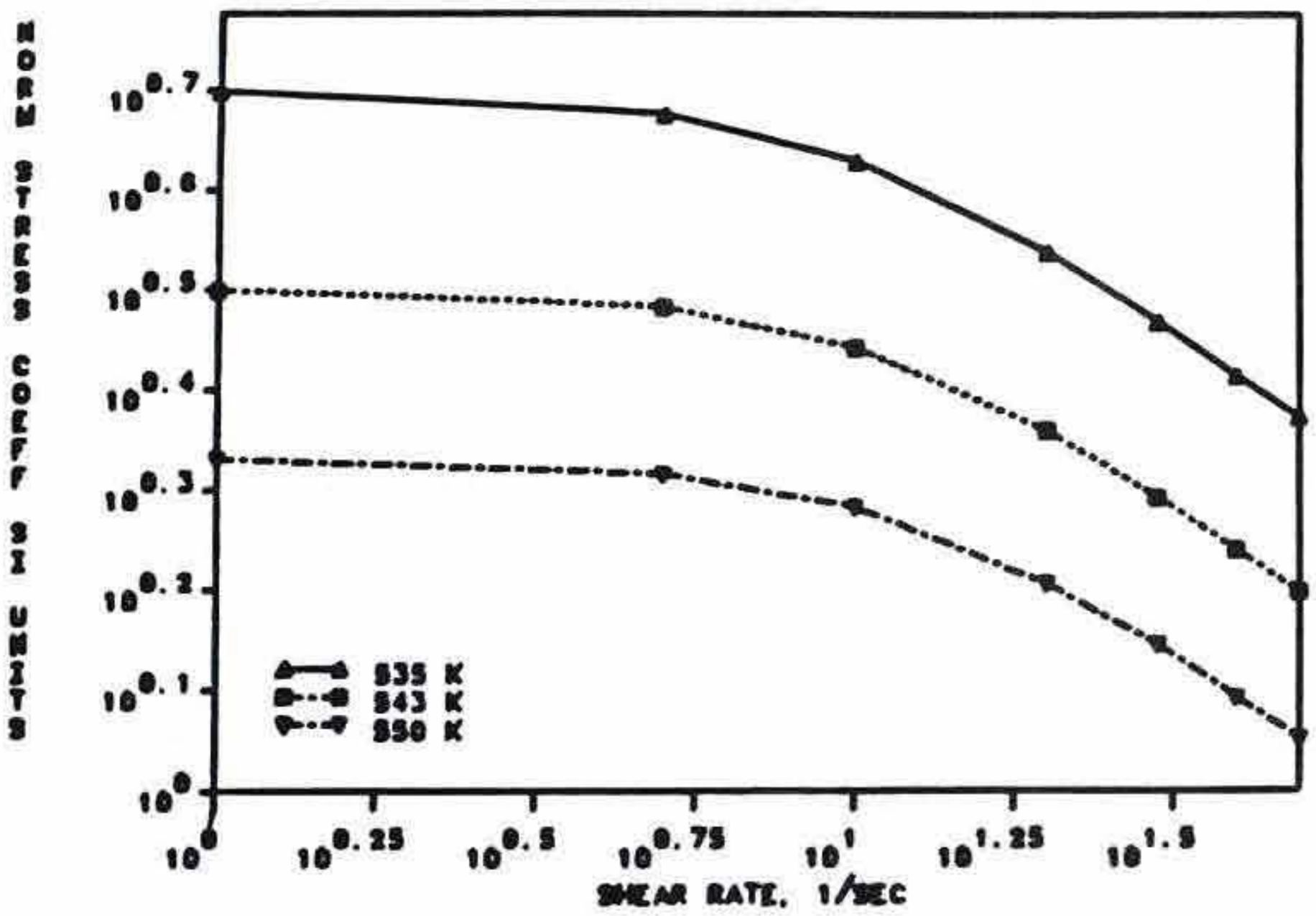

Fig. 15: Normal stress coeff., case (p)

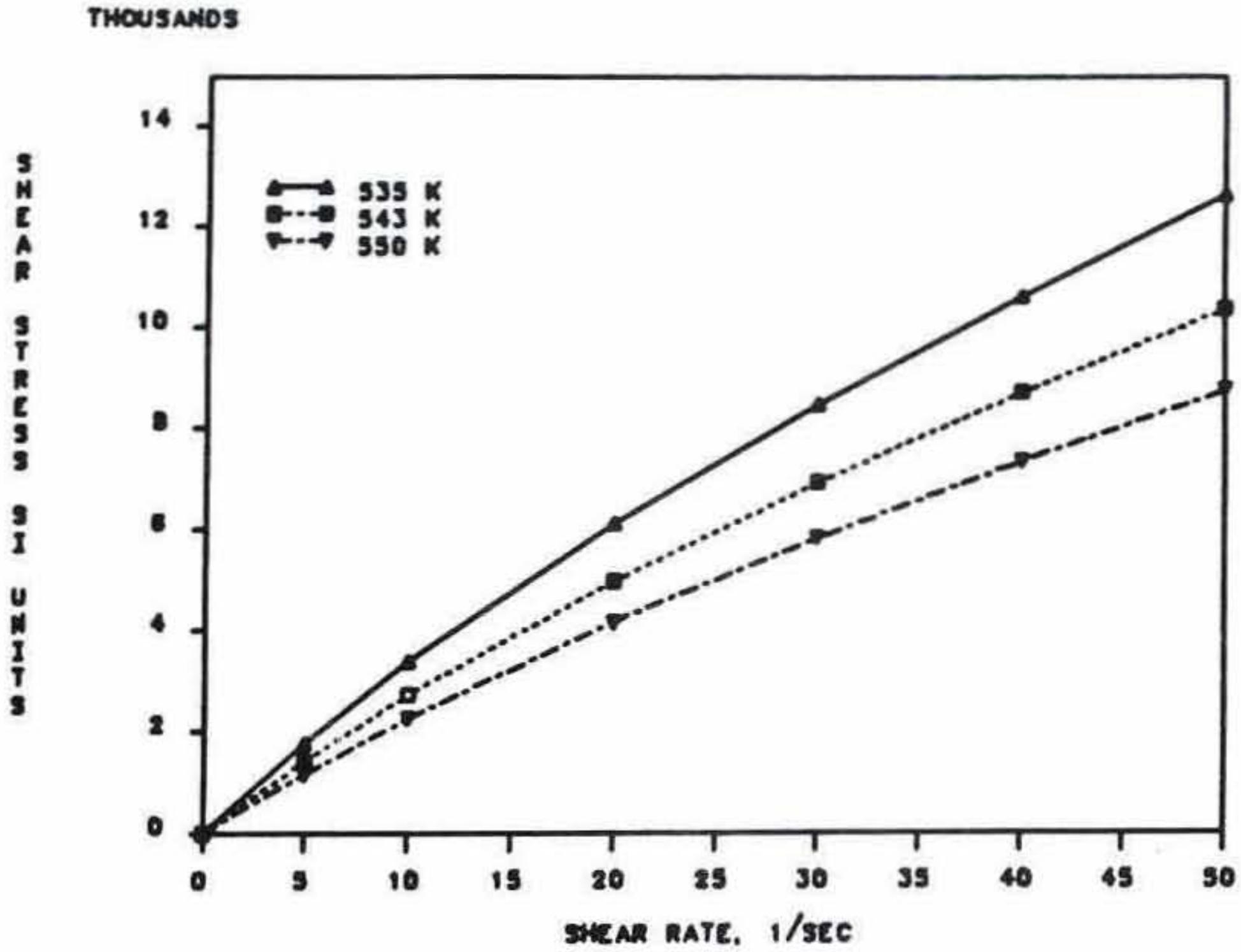

Fig. 16: Shear stress, case (p)

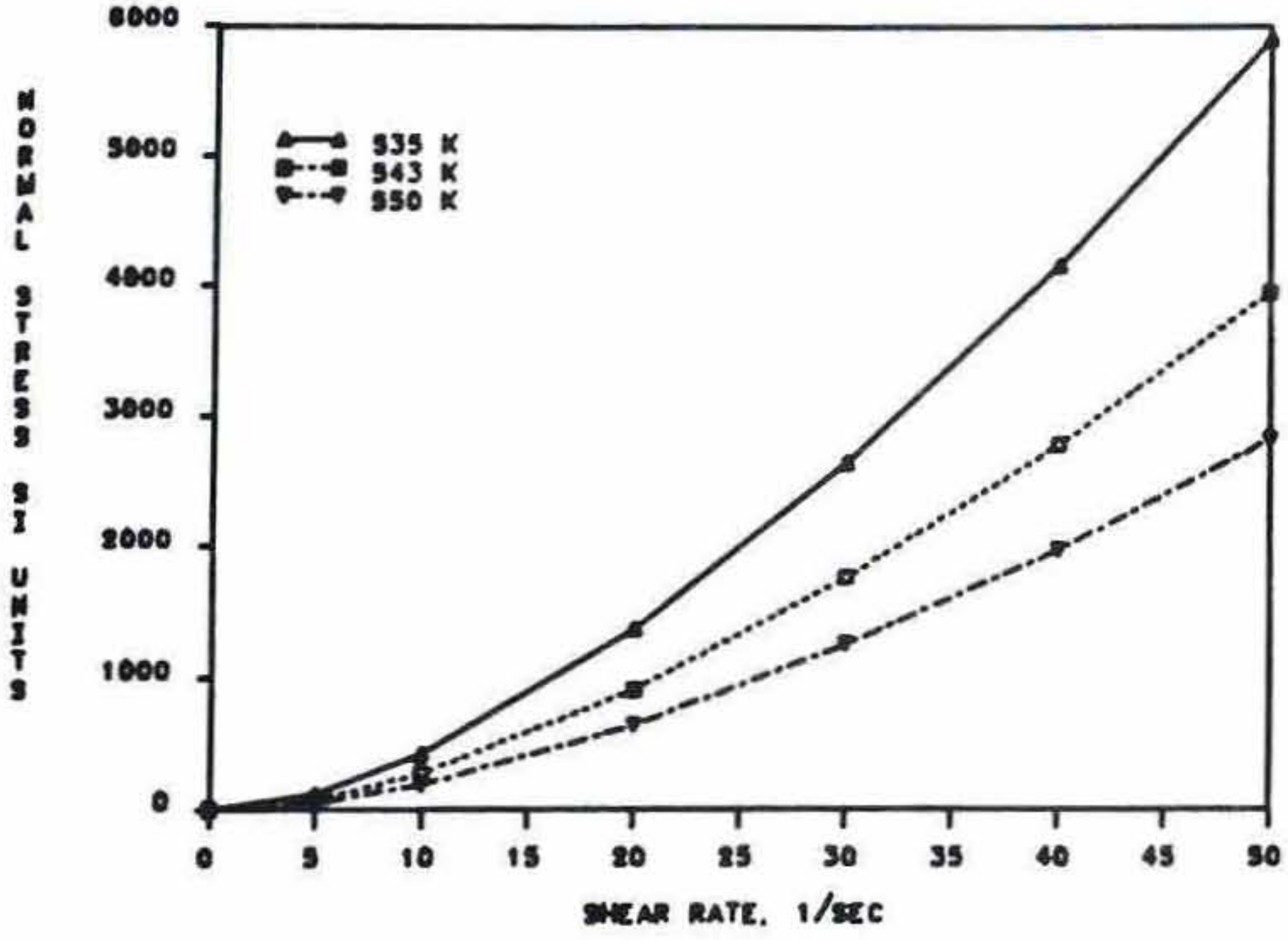

Fig. 17: Normal stress, case (p)

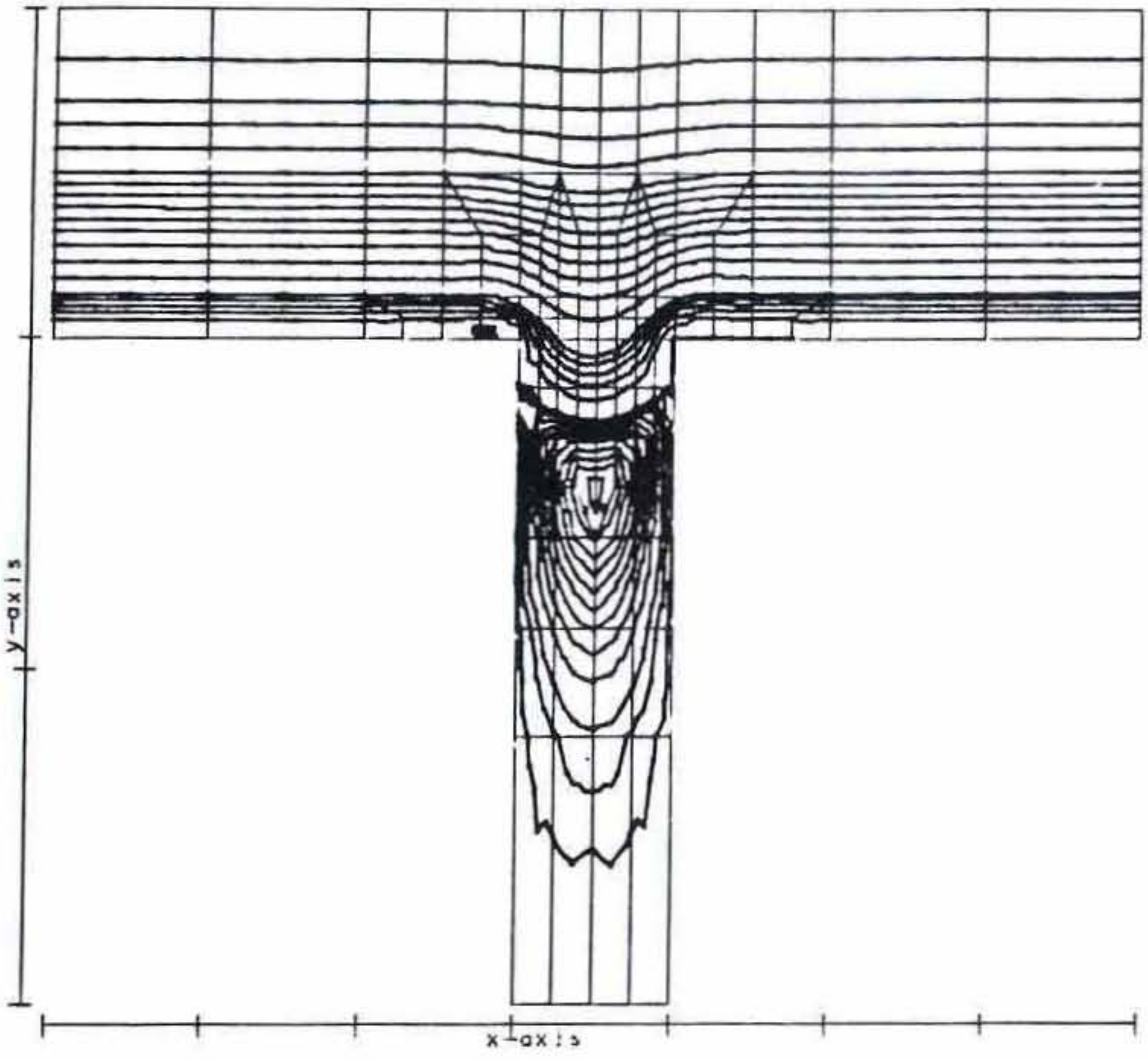

Fig. 18: Streamlines, isothermal, case (c), VETIME2D

Chapter II: Inertial Correction Theory for a Transverse Slot

The Higashitani-Pritchard theory (HP theory, discussed in the Introduction) is valid only under creeping flow conditions, i.e., the theory neglects the inertial terms in the momentum equation. When inertial effects are important (which would be the case for polymer solutions), the hole pressure device can be advantageous in measuring the first normal stress difference (N_1), especially at high shear rates. The cone and plate device (Weissenberg Rheugoniometer), currently being used to measure N_1, cannot handle high shear rates when inertial effects are important, because of secondary flows caused by the centrifugal force. Hence there is a need to include inertial effects in the HP theory, in order to obtain reasonable predictions of the elastic hole pressure at high Reynolds numbers. The hole pressure device is currently being used to measure N_1 at shear rates as high as 3×10^5 s^{-1}, corresponding to Re=15 (by A.S. Lodge at the Rheology Research Center, University of Wisconsin-Madison); such high shear rates are presumably not attainable with the Weissenberg Rheogoniometer on polymer solutions.

Previous Work

Almost all previous attempts at calculating inertial effects have depended on two postulates:

(1) The total hole pressure is the sum of an inertial and an elastic contribution:

$$P_H = P_{IH} + P_{EH} \qquad [2.1]$$

where P_H is the total hole pressure, P_{IH} is the inertial hole pressure (or the inertial correction) and P_{EH} the elastic hole pressure predicted by the HP theory (equation [3]).

(2) The inertial contribution (P_{IH}) can be evaluated from the hole pressure that is exhibited by a Newtonian liquid of equal density and viscosity (at wall shear stress), at the Reynolds number of interest.

One of the earliest papers that uses these two postulates is that by Richards and Townsend (10). These authors used the finite element method to simulate the flow in a transverse slot with an implicit Oldroyd-type model. Lodge and de Vargas (8) used the Newtonian results of Jackson and Finlayson (7) to suggest the following correlation for the inertial hole pressure (P_{IH}):

$$P_{IH} = -0.033\ Re_L \tau_w \qquad [2.2]$$

where Re_L is the hole-based Reynolds number given by:

$$Re_L = \rho H W \dot{\gamma}_w / 4\eta(\dot{\gamma}_w) \qquad [2.3]$$

Here $\dot{\gamma}_w$ is the wall shear rate in undisturbed (fully developed) flow, and $\eta(\dot{\gamma}_w)$ is the viscosity at this shear rate. The other symbols in [2.3] have the meanings described in chapter I. [2.2] reproduces the Newtonian hole pressure data of Jackson and Finlayson (7) accurately for $Re_L \leq 2$, and to within 5% for upto $Re_L \leq 10$; it has been suggested for values of $Re_L \leq 10$ in a later paper by Lodge (11) and used in this range by Malkus and Bernstein (12).

The results of these simulations as well as experiments have shown that when the inertial correction is estimated from postulate (2) (i.e., from the hole pressure of a Newtonian fluid), the resultant elastic hole pressure (P_{EH}) is lower than the predicted theoretical elastic hole pressure (equation [3]) and the agreement worsens as both the Reynolds and Weissenberg numbers increase. This raises the following question: Is the poor agreement due to a failure of the assumptions (A_2-A_4) of the HP theory, or is it because of the failure of postulates (1) and (2) (which have not been theoretically justified)? This question is addressed in the present work; inertial effects are included rigorously in the HP theory, and postulate (1) (equation [2.1]) is justified. The theoretical results obtained also provide indications as to why postulate (2) is unsatisfactory in estimating the inertial contribution, especially at high Reynolds and Weissenberg numbers.

Extended HP theory

The momentum equation is given by (neglecting gravitational terms):

$$Re\ \mathbf{v}.\nabla\mathbf{v} + \nabla P + \nabla.\boldsymbol{\tau} = 0 \qquad [2.4]$$

By assumption A_1 (given in the introduction), the inertial terms in the momentum equation are neglected in the creeping flow HP theory (4), leading to the following equation:

$$\nabla P + \nabla.\boldsymbol{\tau} = 0 \qquad [2.5]$$

[2.5] is transformed to an orthogonal curvilinear coordinate system, and assumptions A_2-A_4 are used to obtain equation [3] of the introduction.

When inertial effects are important (Re>0), symmetry can no longer be expected about the hole centerline. This is especially clear from the experimental flow visualizations and computations of Cochrane, Walters and Webster [13]. Hence, in the extended theory, local symmetry and shear flow are postulated along the path of zero slope of the streamlines (path S), which is illustrated in fig. 19.

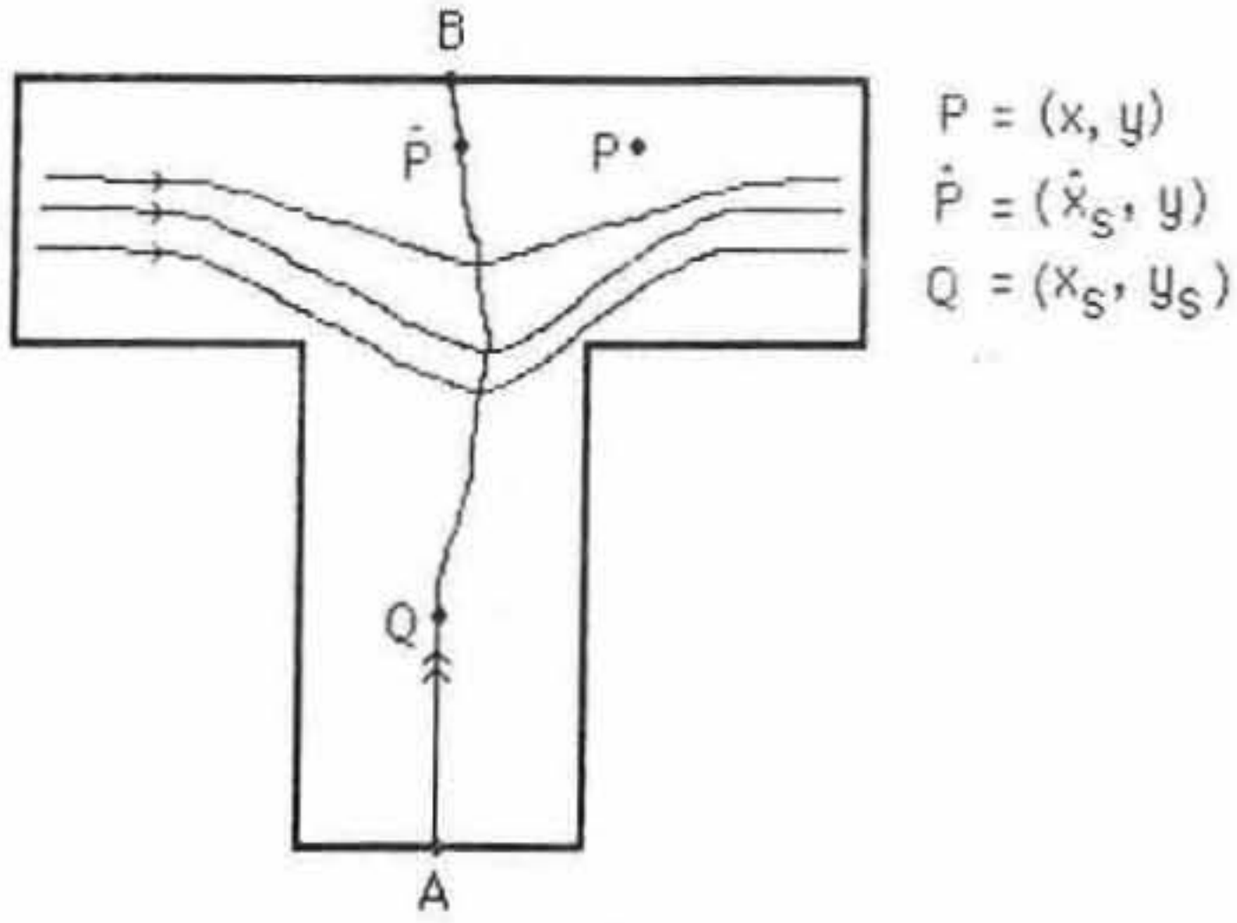

Fig. 19: Path of zero slope of streamlines (Path S)

Path S is defined as that path closest to the hole centerline along which the streamlines have a zero slope at every point with respect to the Cartesian coordinate system. It is assumed that a continuous path S is identifiable, although this need not always be true in the vortex region. The results of [13] show that the effect of inertia is to displace path S beyond the hole centerline in the flow direction.

To formulate the extended HP theory along path S, the isotropic pressure term in [2.4] is split into inertial and elastic parts (P_I and P_E

respectively):

$$P = P_I + P_E \qquad [2.6]$$

The definitions of P_I and P_E are given in Appendix B; it is to be noted that P_I and P_E individually depend on the path S while P, the pressure, does not. These definitions ensure that [2.6] holds along the entire domain; along path S in particular, the following equations must hold:

$$Re\ (\mathbf{v}.\nabla\mathbf{v})_S + \nabla P_{I,S} = 0 \qquad [2.7]$$

$$\nabla P_{E,S} + (\nabla.\boldsymbol{\tau})_S = 0 \qquad [2.8]$$

The subscript S in [2.7] and [2.8] (and the equations that follow) indicates that the variables are to be evaluated along path S. [2.7] and [2.8] follow from the definitions given in Appendix B, and provide the basis for the extended HP theory. The similarity of [2.8] and [2.5] suggests the following definition of the elastic hole pressure:

$$P_{EH} = (P_E + \tau_{yy})_B - (P_E + \tau_{yy})_A \qquad [2.9]$$

where the subscripts B and A refer to the points B and A in fig. 1. Assumptions A_2 to A_4 are now modified to hold along path S, instead of the hole centerline. Further, assumption A_4 is now modified to read :

$$\partial(P_E + \tau_{11})_S/\partial q_1 = 0 \qquad [2.10]$$

Along path S, the 1-direction corresponds to the x-direction. The modification in [2.10] is that P has been replaced by P_E. From [2.6], the following equation can be obtained:

$$\partial P/\partial x = \partial P_I/\partial x + \partial P_E/\partial x \qquad [2.11]$$

Along path S, if the assumption of symmetry is satisfied, [2.7] indicates that $\partial P_{I,S}/\partial x = 0$; hence [2.11] reduces to the following equation if symmetry exists:

$$\partial P_{E,S}/\partial x = \partial P_S/\partial x \qquad [2.12]$$

[2.12] shows that assumption A_4 of the creeping flow theory, and its modification, represented by [2.10], are equivalent if symmetry exists along path S. The modified assumptions of the extended HP theory are now restated as follows:

(A_2) The streamlines are locally symmetric along path S.

(A_3) Unidirectional shear flow exists (and $\partial\tau_{12}/\partial q_1=0$) along path S.

(A_4) $\partial(P_E+\tau_{11})_S/\partial q_1 = 0$, along path S.

Equation [2.8] is transformed to an orthogonal curvilinear coordinate system along path S, in the same way that [2.5] is transformed in the creeping flow theory. Using assumptions A_2 to A_4 now leads to the following equation for the theoretical elastic hole pressure:

$$P_{EH} = -\int_0^{\tau_B} N_1/2\tau_{12}\, d\tau_{12} \qquad [2.13]$$

P_{EH} is the elastic hole pressure defined by [2.9]. [2.13] is the theoretical elastic hole pressure; it is the solution of [2.8] subject to the assumptions A_2 to A_4. In order to check the validity of these assumptions, the exact (or computed) solution of [2.8] could be obtained by directly integrating it along the path of zero slope. Alternatively, equation [2.7] could be integrated along path S, to obtain the following equation for the inertial hole pressure (P_{IH}):

$$P_{IH} = P_{I,B} - P_{I,A} = - Re \int_{(A)}^{(B)} \{u[\partial u/\partial x\, dx + \partial v/\partial x\, dy]\}_S \qquad [2.14]$$

In [2.14], u and v are the x and y- components of the velocity. The integral is evaluated along path S (as shown by the subscript S) with the limits (A) and (B) indicating that the values of x and y at these points are to be used. [2.14] reduces to the following equation if path S coincides with the hole centerline (in which case $(dx)_S=0$) or if local symmetry exists along path S (i.e., $(\partial u/\partial x)_S=0$):

$$P_{IH}= -Re \int_{y_A}^{y_B} (u\partial v/\partial x)_S\, dy_S \qquad [2.15]$$

From [2.4], [2.6] to [2.9], and [2.14], the following equation is obtained:

$$P_{EH} = P_H - P_{IH} \qquad [2.16]$$

[2.16] provides the justification for postulate (1) (i.e., equation [2.1]) and is the exact solution of [2.8]. Equations [2.13] to [2.16] represent the

end point of this analysis. [2.13] is the theoretical elastic hole pressure, [2.14] the inertial correction, and [2.16] the computed elastic hole pressure. The extent of agreement between [2.13] and [2.16] depends only on the validity of the assumptions A_2 to A_4, which are the same as in the creeping flow theory. Since assumption A_1 is no longer needed, the conclusion is that inertial effects have been included exactly in the extended HP theory.

Discussion of the Extended HP theory

When inertial effects are important, assumption A_2 (local symmetry along path S) is likely to dominate the error in the extended HP theory; the results of Webster (6) lead us to conclude that this would tend to increase the computed (or actual) elastic hole pressure (given by [2.16]) above the theoretical prediction [2.13]; i.e., there would be a negative error in the theory. This is especially true when inertia is large relative to elasticity. Hence it would seem necessary to include a correction factor for asymmetry in the extended HP theory. This could be done using the approach of Webster (6), by forcing the theory to be exact for a Newtonian liquid. Two additional correction factors are defined as follows:

$$P_{SH} = \int_{(A)}^{(B)} \{(\partial^2 v/\partial x^2 + \partial^2 v/\partial y^2)dy\}_S \qquad [2.17]$$

$$P_{PH} = \int_{(A)}^{(B)} \{(\partial^2 u/\partial x^2 + \partial^2 u/\partial y^2)dx\}_S \qquad [2.18]$$

The integrals in [2.17] and [2.18] are evaluated along path S, from point A to point B. [2.16] is modified to include these additional correction factors, and the elastic hole pressure is defined as follows:

$$P_{EH} = P_H - P_{IH} - P_{SH} - P_{PH} \qquad [2.19]$$

P_{IH} is the inertial correction given by [2.14]. P_{SH} can be viewed as a correction factor for asymmetry (assumption A_2), and P_{PH}, for assumption A_4. It is easily seen that with these additional correction factors, [2.19] predicts a zero elastic hole pressure for Newtonian liquids, in accordance with the theory [2.13]. It is to be noted that while P_{IH} is a rigorous correction (for assumption A_1, i.e., for inertial effects), P_{SH} and P_{PH} are not so for the non-Newtonian case.

The current theory uses postulate (2), i.e., a Newtonian hole pressure as a correction factor, according to the following:

$$P_{EH} = P_H - P_{H,N} \qquad [2.20]$$

The Newtonian hole pressure ($P_{H,N}$) can be viewed as follows:

$$P_{H,N} = P_{IH,N} + P_{SH,N} + P_{PH,N} \qquad [2.21]$$

where the subscript N indicates a Newtonian velocity profile. The three terms on the right hand side of [2.21] are evaluated from [2.14], [2.17] and [2.18] respectively, for the Newtonian profile. [2.19] requires that the above correction factors be evaluated from the actual, rather than

the Newtonian, velocity profile. A comparison of the Newtonian velocity profile with the elastic solutions shows two important differences:

(a) The Newtonian velocity profile quickly loses symmetry about path S, as the Reynolds number increases. In an elastic fluid, the opposing effect of elasticity preserves some of this symmetry (13). Asymmetry due to inertia tends to cause a greater pressure at point B than at point A (6), i.e., asymmetry opposes the inertial effect. Hence $P_{SH,N}$ and P_{SH} are positive numbers; this implies that:

$$P_{SH,N} > P_{SH} \qquad [2.22]$$

i.e., the Newtonian profile has a correction factor for asymmetry that is larger than required.

(b) A second important difference between Newtonian and elastic velocity profiles is that the streamlines in elastic flow tend to dip deeper into the hole as the elasticity increases, as seen from the lower positioning of the primary vortex in the hole for the elastic case (13); for a Newtonian case, the vortex tends to move in the opposite direction as the Reynolds number increases (7,12). This is observed both experimentally (13) and computationally (7,12,13), although the computed results are less dramatic than the experimental ones. The implication of this observation is that the curvature of the streamlines along path S in elastic flow is higher than in the Newtonian case, and the difference is greater as Re and We increase. In appendix C, it is proved that the inertial contribution, as given by [2.14], is directly proportional to the curvature of the streamlines in the special case of a

symmetric velocity profile, i.e.,

$$(\partial P_I/\partial y)_S = - Re\ (u^2\ d^2y/dx^2)_S \qquad [2.23]$$

This implies that $|P_{IH,N}| < |P_{IH}|$, or, since P_{IH} is a negative quantity:

$$P_{IH,N} > P_{IH} \qquad [2.24]$$

The effects of both the errors [2.22] and [2.24] caused by the Newtonian profile tend to produce a positive error in the theory, i.e., they tend to reduce the computed or actual P_{EH} below the theoretical P_{EH}; these errors increase as Re and We increase. Thus the conclusion is that [2.22] and [2.24] provide the reasons for the failure of the Newtonian hole pressure as a correction factor at higher Re.

Conclusion

Inertial effects have been successfully included in the HP theory. The extended HP theory proposed in this work provides insight as to why the current technique of using a Newtonian hole pressure as the inertial correction is unsatisfactory, and suggests that the inertial contribution, evaluated from the actual velocity profile, is a function of both Re and We. Extensive computation is needed to device a suitable correction factor for asymmetry in the extended HP theory proposed in this work ([2.17] is exact only for the Newtonian case) and also to correlate the inertial correction as a function of geometry, elasticity, Re, and wall shear stress.

References

{1} J.M. Broadbent, A.Kaye, A.S.Lodge, D.G.Vale, Nature, 217 (1968) 55-56.

{2} R.B.Bird, R.C.Armstrong and O.Hassager, Dynamics of Polymeric Liquids, Volume 1, sec. 3.4 (pp. 97-101), Wiley, New York, 1977.

{3} R.I.Tanner and A.C.Pipkin, Trans. Soc. Rheol., 13 (1969) 471-484.

{4} K.Higashitani and W.G.Pritchard, Trans. Soc. Rheol., 16 (1972) 687-696.

{5} D.G.Baird, J. Appl. Polym. Sci., 20 (1976) 3155-73.

{6} M.F.Webster, Rheol. Acta, 23 (1984) 582-590.

{7} N.R.Jackson and B.A.Finlayson, J. Non-Newtonian Fluid Mech., 10 (1982) Part I: 55-69, Part II: 71-84.

{8} A.S.Lodge and L. de Vargas, Rheol. Acta, 22 (1983) 151-170.

{9} B.A.Finlayson and M.McClelland, Numerical Methods in Heat Transfer, Volume 3, 1985, Chapter 13 (269-287).

{10} G.D.Richards, P.Townsend, Rheol. Acta, 20 (1981) 261-269.

{11} A.S. Lodge, J. Rheology, 27 (1983) 497-501.

{12} D.S. Malkus and B.Bernstein, J. Non-Newtonian Fluid Mech., 16 (1984) 77-116.

{13} T.Cochrane, K.Walters and M.F.Webster, Phil. Trans. Roy. Soc. London, 301 (1981) 163-182.

Appendix A: Evaluation of Theoretical Correction Factors

Evaluation of CF1

The temperature and shear stress at the inlet of the channel are calculated as a function of position (y) using finite element interpolation (quadratic temperature, linear stresses) in the bottom half of the channel, which has a greater degree of refinement than the top half. The parameter y is eliminated between the equations for temperature and stress, to obtain the temperature directly as a function of shear stress ($T(\tau_{12})$, used in [1.18]). The shear stress is used as the independent variable of integration, and the temperature at a given value of the shear stress is calculated from the above function. The shear rate is calculated from the available shear stress and temperature, using [1.11]. The normal stress is then evaluated at the available shear rate and temperature from [1.14]. The integration of [1.18] is done using Simpson's rule. Equation [1.19] is integrated with the viscometric functions ([1.11] and [1.14]) evaluated at the wall temperature only. CF1 is evaluated from [1.20] as the ratio of the nonisothermal to isothermal hole pressures.

Evaluation of CF2

Substituting the viscometric functions [1.11] and [1.14] in [1.21] yields the following equation for the nondimensional hole pressure at a given temperature T':

$$P_H(\dot{\gamma}_B', T') = C \int_0^{\dot{\gamma}_B'} \frac{\dot{\gamma}'[1+n(\lambda_1'(T')\dot{\gamma}')^2]}{2[1+(\lambda_2'(T')\dot{\gamma}')^2]^{(2-n')/2}\,[1+(\lambda_1'(T')\dot{\gamma}')^2]}\, d\dot{\gamma}' \qquad [A.1]$$

where $C = H\psi_{1,0}'(T')/[\eta_0'(T_w')\langle v_x'\rangle]$

The correction factor CF2 is evaluated from [1.22] and [A.1] as follows:

$$CF2 = P_H(\dot{\gamma}_B'(T_w'), T_a')/\, P_H(\dot{\gamma}_B'(T_w'), T_w') \qquad [A.2]$$

T_a' is the average temperature evaluated from [1.24]. The value of $\dot{\gamma}_B'(T_w')$ used as the upper limit in both numerator and denominator of [A.2] is the the wall shear rate at point B calculated from the isothermal VEHEATD solution. The denominator of [A.2] is the isothermal hole pressure, equivalent to [1.19].

Appendix B: Definitions of Inertial and Elastic Pressures

The objective of this section is to define the quantities P_I and P_E uniquely throughout the domain, such that equations [2.6], [2.7] and [2.8] are satisfied along the path of zero slope of the streamlines (path S, shown in fig. 19). The following functions are defined to hold at any arbitrary point (x,y) (fig. 19) in the domain:

$$f_1(x,y) = -Re(u\partial u/\partial x + v\partial u/\partial y) \qquad [B.1]$$

$$f_2(x,y) = -Re(u\partial v/\partial x + v\partial v/\partial y) \qquad [B.2]$$

$$g_1(x,y) = -(\partial \tau_{xx}/\partial x + \partial \tau_{xy}/\partial y) \qquad [B.3]$$

$$g_2(x,y) = -(\partial \tau_{xy}/\partial x + \partial \tau_{yy}/\partial y) \qquad [B.4]$$

The quantities P_I and P_E are now defined in terms of these functions at any point (x,y); in the definitions that follow, the subscript S indicates that the variables are to be evaluated along path S:

$$P_I(x,y) = P_{I,A} + \int_{y_A}^{y} f_2(x_S, y_S)dy_S + \int_{x_A}^{\hat{x}_S} f_1(x_S, y_S)dx_S + \int_{\hat{x}_S}^{x} f_1(\tilde{x}, y)d\tilde{x} \qquad [B.5]$$

$$P_E(x,y) = P_{E,A} + \int_{y_A}^{y} g_2(x_S, y_S)dy_S + \int_{x_A}^{\hat{x}_S} g_1(x_S, y_S)dx_S + \int_{\hat{x}_S}^{x} g_1(\tilde{x}, y)d\tilde{x} \qquad [B.6]$$

In [B.5] and [B.6], $\hat{x}_S$ refers to the x-coordinate of that point on path S whose y-coordinate is y (the point $(\hat{x}_S,y)$ is shown in fig. 19), and $\tilde{x}$ is a dummy variable of integration; x_A and y_A represent the coordinates of the point A in fig. 19; $P_I(x,y)$ and $P_E(x,y)$ are the inertial and elastic

pressures at any point (x,y) in the domain. $P_{I,A}$ and $P_{E,A}$ are arbitrary constants representing the inertial and elastic pressures at point A, and satisfying the condition:

$$P_{I,A} + P_{E,A} = P_A \qquad [B.7]$$

where P_A is the pressure at point A.

It is easily verified that [B.5] and [B.6] satisfy [2.6], [2.7] and [2.8].

Appendix C: Proof that inertial correction is proportional to curvature of streamlines

The slope of a streamline at any point is given by:

$$dy/dx=v/u \qquad [C.1]$$

Differentiating [C.1] with respect to x and using the equation of continuity yields:

$$u^2d^2y/dx^2 = (u\partial v/\partial x + v\partial v/\partial y) - dy/dx\,(u\partial u/\partial x + v\partial u/\partial y) \qquad [C.2]$$

Comparing [C.2] with [2.7] (which is valid along path S) yields:

$$-Re(u^2d^2y/dx^2)_S = (\partial P_I/\partial y)_S - (dy/dx)_S(\partial P_I/\partial x)_S \qquad [C.3]$$

The subscript S refers to path S, which is defined such that:

$$(dy/dx)_S = 0 \qquad [C.4]$$

Hence [C.3] reduces to:

$$(\partial P_I/\partial y)_S = -Re(u^2d^2y/dx^2)_S \qquad [C.5]$$

If symmetry exists along path S, $(\partial P_I/\partial x)_S = 0$; the inertial hole pressure is then given by integrating [C.5] along path S. Equation [C.5] shows that

the inertial correction is proportional to the curvature of the streamlines along path S, for the special case of a symmetric velocity profile.

Comparison to Newtonian Hole Pressure

[C.5] makes possible a comparison between postulate (2), which uses a Newtonian hole pressure as the inertial correction, and equation [2.15] (which reduces to [C.5], as shown above) for small Re, when path S is close to the centerline. The y-component of the momentum equation in Newtonian flow (as denoted by subscript N) is given by:

$$Re(u_N \partial v_N/\partial x + v_N \partial v_N/\partial y)_S + (\partial P_N/\partial y)_S = \mu(\partial^2 v_N/\partial x^2 + \partial^2 v_N/\partial y^2)_S \qquad [C.6]$$

When Re is small, path S is assumed to be close to the centerline; further local symmetry is also assumed along the centerline. Under these conditions, $(\partial^2 v_N/\partial x^2)_S$ and $(\partial^2 v_N/\partial y^2)_S$ are both identically zero ($(\partial^2 v_N/\partial x^2)_S$ is zero because v_N must be an anti-symmetric function of x about the hole centerline if the streamlines are symmetric, and hence must pass through zero curvature with respect to x at the centerline; this is also seen from the following finite difference expression:

$$(\partial^2 v_N/\partial x^2)_S = (v_{N,\,i+1} - 2\, v_{N,\,i} + v_{N,\,i-1})/2\Delta x \qquad [C.7]$$

where i refers to the hole centerline. Under conditions of symmetry of streamlines, $v_{N,i}=0$ and $v_{N,i+1} = -v_{N,i-1}$; hence it follows that $(\partial^2 v_N/\partial x^2)_S=0$. $(\partial^2 v_N/\partial y^2)_S$ also equals zero because v_N is identically zero

along the hole centerline if symmetry exists). Therefore [C.6] reduces to:

$$(\partial P_N/\partial y)_S = -Re(u_N \partial v_N/\partial x)_S \qquad [C.8]$$

[C.8] is similar to [2.15], which is valid under conditions of local symmetry; hence [C.8] can be reduced to an equation similar to [C.5] by an identical derivation:

$$(\partial P_N/\partial y)_S = -Re\{u_N{}^2(d^2y/dx^2)_N\}_S \qquad [C.9]$$

[C.9] shows that under conditions of local symmetry about the hole centerline, a Newtonian hole pressure (which is the inertial correction as given by postulate (2)) is proportional to the curvature of the streamlines in Newtonian flow; [C.5] shows that the inertial correction proposed in the present work (under conditions of local symmetry, as given by [2.15]) is proportional to the curvature of the streamlines in elastic flow. Since the curvature of the streamlines along path S in elastic flow is found to be higher than that in Newtonian flow (as seen from the lowering of the primary vortex in elastic flow), [C.5] would yield a higher inertial correction than [C.9].